# Oceanic response to Pliensbachian and Toarcian magmatic events: Implications from an organic-rich basinal succession in the NW Tethys

S. Neumeister [a,*], R. Gratzer [a], T. J. Algeo [b], A. Bechtel [a], H.-J. Gawlick [a], R. J. Newton [c], R. F. Sachsenhofer [a]

[a] *Department of Applied Geosciences and Geophysics, Montanuniversitaet Leoben, Peter-Tunner-Str. 5, A-8700 Leoben, Austria*

[b] *Department of Geology, University of Cincinnati, Cincinnati, OH 45221, USA*

[c] *The School of Earth and Environment, The University of Leeds, Woodhouse Lane, Leeds, West Yorkshire, LS2 9JT, UK*

* Corresponding author at: Department of Applied Geosciences and Geophysics, Montanuniversitaet Leoben, Peter-Tunner-Str. 5, A-8700 Leoben, Austria. Tel.: +43 664 5049925.
E-Mail address: st.neumeister@hotmail.com (Stefan Neumeister).

***Abstract***

The Bächental bituminous marls (Bächentaler Bitumenmergel) belonging to the *Sachrang Member* of the Lower Jurassic *Middle Allgäu Formation* were investigated using a multidisciplinary approach to determine environmental controls on the formation of organic-rich deposits in a semi-restricted basin of the NW Tethys during the Early Jurassic. The marls are subdivided into three units on the basis of mineralogical composition, source-rock parameters, redox conditions, salinity variations, and diagenetic processes. Redox proxies (e.g., pristane/phytane ratio; aryl isoprenoids; bioturbation; ternary plot of iron, total organic carbon, and sulphur) indicate varying suboxic to euxinic conditions during deposition of the Bächental section. Redox variations were mainly controlled by sea-level fluctuations with the tectonically complex bathymetry of the Bächental basin determining watermass exchange with the Tethys Ocean. Accordingly, strongest anoxia and highest total organic carbon content (up to 13%) occur in the middle part of the profile (upper *tenuicostatum* and lower *falciferum* zones), coincident with an increase in surface-water productivity during a period of relative sea-level lowstand that induced salinity stratification in a stagnant basin setting. This level corresponds to the time interval of the lower Toarcian oceanic anoxic event (T-OAE). However, the absence of the widely observed lower Toarcian negative carbon isotope

excursion in the study section questions its unrestricted use as a global chemostratigraphic marker. Stratigraphic correlation of the thermally immature Bächental bituminous marls with the Posidonia Shale of SW Germany on the basis of $C_{27}/C_{29}$ sterane ratio profiles and ammonite data suggests that deposition of organic matter-rich sediments in isolated basins in the Alpine realm commenced earlier (late Pliensbachian *margaritatus* Zone) than in regionally proximal epicontinental seas (early Toarcian *tenuicostatum* Zone). The late Pliensbachian onset of reducing conditions in the Bächental basin coincided with an influx of volcaniclastic detritus that was possibly connected to complex rifting processes of the Alpine Tethys and with a globally observed eruption-induced extinction event. The level of maximum organic matter accumulation in the Bächental basin corresponds to the main eruptive phase of the Karoo-Ferrar large igneous province (LIP), confirming its massive impact on global climate and oceanic conditions during the Early Jurassic. The Bächental marl succession is thus a record of the complex interaction of global (i.e., LIP) and local (e.g., redox and salinity variations, basin morphology) factors that caused reducing conditions and organic matter enrichment in the Bächental basin. These developments resulted in highly inhomogeneous environmental conditions in semi-restricted basins of the NW Tethyan domain during late Pliensbachian and early Toarcian time.

***Keywords:*** Bächental marl; Sachrang Member; Allgäu Formation; oceanic anoxic event; anoxia; sea level; carbon isotopes; Northern Calcareous Alps; Karoo-Ferrar; Alpine Tethys

## 1. Introduction

The early Toarcian was characterized by the deposition of organic-rich sediments in marine systems globally (e.g., Jenkyns, 1985, 1988; Jenkyns et al., 2002; Pearce et al., 2008), although the main controls on organic matter (OM) production and preservation at that time remain controversial. Widespread anoxia in epicontinental areas of the western Tethyan region (i.e., depositional area of the Posidonia Shale) has been attributed to a surface-water layer with reduced salinity that caused intensified water-column stratification (Praus and Riegel, 1989; Littke et al., 1991; Sælen et al., 1996). Other possible influences include minor sea-level fluctuations that controlled watermass exchange and, hence, dissolved oxygen levels in semi-restricted basins within the western European epicontinental sea (Röhl et al., 2001; Schmid-Röhl et al., 2002; Frimmel et al., 2004). In contrast, Jenkyns (1985, 1988; a summary is given by Jenkyns, 2010) postulated upwelling connected with the T-OAE of global scale

for causing the high rates of organic carbon accumulation in lower Toarcian strata. Tsikos et al. (2004a) found that the definition of Toarcian organic-rich sediments on the basis of their stratigraphic distribution is problematic as preservation and dilution of OM was affected by local variations in depositional and diagenetic conditions.

Changes in global climate during the Early Jurassic created oceanic conditions that were generally conducive to development of anoxia. Significant climatic warming had begun with release of large quantities of greenhouse gases during the CAMP eruptions at ~201 Ma (Marzoli et al., 1999; Whiteside et al., 2007). An interval of relative global cooling during the late Pliensbachian (Price, 1999; Morard et al., 2003; Dera et al., 2010) was followed by eruption of two large igneous provinces in the Early Jurassic: (1) the Karoo LIP at ~183 Ma (Svensen et al., 2007, 2012; Sell et al., 2014), and (2) the Ferrar LIP at ~184-183 Ma (Encarnación et al., 1996; Minor and Mukasa, 1997). These eruptions served to induce further climatic warming from the Pliensbachian/Toarcian boundary onwards, leading to "greenhouse Earth" conditions (Palfy and Smith, 2000; Weissert, 2000; Jenkyns, 2003). The prevailing subtropical climate was accompanied by an accelerated hydrological cycle with heavy monsoonal rainfalls and intense continental weathering that triggered an extensive supply of nutrients for ocean-surface waters, enhancing primary productivity (Parrish and Curtis, 1982; Parrish, 1993; Cohen et al., 2004). In addition, rifting of the Alpine Tethys was associated with several regional magmatic pulses during late Triassic to middle Jurassic time (Mohn et al., 2010; Decarlis et al., 2013). Oceanic break-up in the Penninic realm occurred in the Pliensbachian-Toarcian (Ratschbacher et al., 2004). These environmental changes operated in concert to produce conditions favourable to marine anoxia and black shale accumulation variably at global to local scales during the Early Jurassic.

Several studies have documented significant variation in total organic carbon (TOC) levels within lower Toarcian deposits of northern and southern Europe (see Jenkyns, 2010, for references). Whereas black shales deposited in epicontinental settings in Britain, France, and Germany reach peak TOC contents of up to 20% (e.g., Küspert, 1982; Jenkyns and Clayton, 1997; Röhl et al., 2001), coeval sediments of the pelagic Tethyan realm generally contain smaller amounts of OM (<5 %; e.g., Jenkyns, 1985; 1988; Sabatino et al., 2009, 2013). Bituminous marls of Early Jurassic age (Bächentaler Bitumenmergel) are found in the Bächental valley of the Northern Calcareous Alps (Fig. 1.A). The Bächental basin was located in the NW part of the Tethys Ocean during the Toarcian (Figs. 1.B-C). A detailed investigation of the depositional environment of the Bächental bituminous marls as well as exact data regarding the onset and duration of its accumulation are lacking. However,

exceptionally high TOC contents (13 %) and an onset of OM accumulation during the Pliensbachian were reported by Kodina et al. (1988).

A multidisciplinary approach with high sample resolution was applied to the investigation of the Bächental bituminous marls. The use of a variety of proxies yielded information on source and thermal maturity of OM, redox conditions, salinity, water-column stratification, sea-level fluctuations, diagenetic processes, and volcanic influences. A comprehensive interpretation of these data permits the establishment of an overall model for the deposition of the Bächental bituminous marls. In addition, new findings regarding the age of marl accumulation facilitate stratigraphic correlation of lower Toarcian deposits from Alpine and epicontinental settings. The present study provides insights concerning the role of global events (e.g., Karoo and Ferrar LIP magmatism, opening of the Atlantic Ocean) as well as the influence of local basinal factors (e.g., redox and salinity variations) on OM accumulation in semi-restricted basins (e.g., Bächental basin) of the northwestern Tethyan domain during the late Pliensbachian and early Toarcian.

## 2. Geological setting and samples

The investigated section is situated in the Bächental valley, which is part of the Karwendel Mountains of northern Tyrol (Fig. 1.A; GPS: 47°30'31.38"N; 11°37'46.00"E). In this area, lithostratigraphic units of Triassic to Jurassic age belonging to the Lechtal nappe of the Bavaric Unit, a tectonic domain of the Northern Calcareous Alps, are exposed.

The paleogeography of the depositional area of the Bächental bituminous marls (Figs. 1.B-C) was controlled by extensional tectonics, related to late Hettangian rifting and Toarcian oceanic break-up in the Penninic realm (e.g., Ratschbacher et al., 2004). During late Hettangian to Sinemurian time (Schlager and Schöllnberger, 1973) the final configuration of the roughly north-south trending Bächental basin with half-graben geometry, a depocenter located in the northern part of the basin, tilt block tectonics and antithetic step faults were established (Spieler and Brandner, 1989; Fig. 1.D). The distribution of bituminous marls (Fig. 1.E) deposited during the early Toarcian was limited to the poorly ventilated deepest part of the Bächental basin (Spieler and Brandner, 1989).

The study section has an overall thickness of 35.54 m (Fig. 2) and is well exposed in large parts due to its position in an open-pit mine. At its base, limestone beds with a total thickness of 4.00 m occur. These strata are assigned to the *Scheibelberg Formation* (Sinemurian to Pliensbachian) and were deposited in water depths of several hundred meters

at the transition of distal slope to basin (Spieler and Brandner, 1989). Directly above a 0.25-m-thick weathered mudstone, the Bächental bituminous marls of the upper Pliensbachian to lower Toarcian *Sachrang Member* of the *Middle Allgäu Formation* (Tollmann, 1976a; Ebli, 1991; Ebli et al., 1998; Gawlick et al., 2009; this study) are exposed with a total thickness of 23.70 m. The alternating sequence of limestone and marl with a thickness of 4.69 m forming the top of the succession belongs to the *Upper Allgäu Formation* (upper Toarcian to early Middle Jurassic; Spieler and Brandner, 1989). The dating of the Bächental bituminous marls to the Toarcian was originally based on the occurrence of *Harpoceras* sp. (Klebelsberg, 1935). Kodina et al. (1988) inferred that bituminous marl sedimentation began during the late Pliensbachian based on the occurrence of *Arieticeras* sp. and *Arieticeras* sp. or *Leptaleoceras* sp. near the base of the marls. This is consistent with the presence of *Cleviceras exaratum* in the middle part of the section (13.40 m; Fig. 2), a taxon associated with the early Toarcian *falciferum* Zone. A late Pliensbachian age (*margaritatus* Zone) for the base of the *Sachrang Member* in the Bächental basin is further supported by correlations based on $C_{27}/C_{29}$ sterane ratios (Fig. 2; see Section 5.3.1 for discussion). At its type locality in Bavaria, deposition of the *Sachrang Member* commenced at the base of the *tenuicostatum* Zone and continued through the entire early Toarcian (Ebli et al., 1998).

Samples were collected from fresh exposures in a trench that was dug up to 4 m deep. A total of 68 samples was collected for geochemical analyses (Fig. 2). The *Scheibelberg Formation* at the base of the study succession is represented by six samples. The *Sachrang Member*, including a basal mudstone, bituminous marls, and a 1-meter-thick debrite layer (Fig. 2), is represented by 52 samples resulting in an average sampling interval of ca. 0.50 m. Ten samples at intervals of 0.10 to 0.90 m were collected from the *Upper Allgäu Formation* at the top of the section.

## 3. Analytical methods

A total of 28 thin sections were made for analyses via transmitted light microscopy. Polished blocks of 12 samples were prepared for maceral analyses that were performed with a Leica MPV microscope.

Total carbon (TC) and sulphur (S) contents were measured with a Leco 300 CSTM analyser. For the determination of total organic carbon (TOC) sample material was pre-treated with concentrated hydrochloric acid to remove the carbonate-bound carbon. Total inorganic carbon (TIC = TC – TOC) was used to calculate calcite equivalent percentages ($Cc_{eq}$ = TIC x

8.33). Rock Eval pyrolysis was carried out using a Delsi Rock Eval RE II+ instrument. By means of this method the amount of free hydrocarbons ($S_1$; mg HC/g rock) released at a constant temperature as well as the amount of pyrolysate ($S_2$; mg HC/g rock) generated from non-volatile OM during subsequent gradual heating of the rock powder in a helium stream can be measured. These values are used to calculate the production index [$PI = S_1/(S_1 + S_2)$] and the hydrogen index [$HI = (S_2/TOC) \times 100$]. The temperature of maximum hydrocarbon generation ($T_{max}$) can be used as maturity indicator.

X-ray diffraction (XRD) was carried out using Philips X-pert equipment with the following measuring conditions: [i] bulk samples, 2 to 65° 2θ, random powder mount (29 samples); [ii] clay mineral analysis of clay-rich samples, oriented powder mounts (smear on glass; Vortisch, 1982), 2 to 38° 2θ, untreated, ethylene glycol-treated, heat-treated, 350 °C/2 h, 550 °C/2 h (2 samples); [iii] bulk samples, 25 to 35° 2θ, random powder mount (21 samples). A rough quantification of the amount of diagenetic carbonate (unit: peak area) was established using the carbonate peaks between 30.0 and 31.2° 2θ in XRD diffractograms.

Inorganic carbon ($\delta^{13}C_{carb}$) and oxygen isotope ($\delta^{18}O_{carb}$) measurements were carried out for all samples. Measurements were performed by adding 100 % $H_3PO_4$ to samples heated at 70 °C in an online system (Gasbench II with carbonate option). Analysis was carried out with a ThermoFisher DELTA V isotope ratio mass spectrometer (Delta V IRMS). The results are reported relative to the Vienna Pee Dee Belemnite (VPDB) standard. Reproducibility was better than 0.2‰. All samples were analysed for their organic carbon isotope composition at the University of Leeds using an Elementar Pyrocube coupled to an Isoprime IRMS. Samples were weighed into tin capsules in sufficient quantity to produce peaks of between 1 and 10nA and combusted at 1150 °C in a helium stream (CP grade) enriched with pure oxygen (N5.0). The resulting gases were passed over tungstic oxide (also at 1150 °C) and excess oxygen and water removed using copper wires held at 850 °C and Sicapent respectively. All solid reagents were sourced from Elemental Microanalysis, UK, and all gases were sourced from BOC, UK. $CO_2$ was separated from other gases using a temperature controlled adsorption/desorption column. The $\delta^{13}C$ of the sample is derived from the integrated mass 44, 45 and 46 signals from the pulse of sample $CO_2$, compared to those in an independently introduced pulse of $CO_2$ reference gas (CP grade). Samples were run in batches of 12-16 bracketed by in-house C4 sucrose and urea standards. These were assigned values of -11.93 ± 0.24 and -46.83 ± 0.22‰ respectively based on 10 replicate analyses and calibration using LSVEC lithium carbonate (-46.479‰), IAEA-CH7 polyethylene (-31.83‰), IAEA-CH6 sucrose (-10.45‰) and IAEA-CO1 Carrara marble (2.48‰). Samples were batch corrected

using a simple linear equation. Analysis of the C-isotopic composition of acyclic isoprenoids was performed using a Trace GC Ultra attached to a Delta V IRMS via a combustion interface (GC IsoLink) and an autodilution unit (ConFlow IV), all from Thermo-Fisher. For calibration, a $CO_2$ standard was injected at the beginning and end of each analysis. The GC coupled to the IRMS was equipped with the column described above and the temperature program was the same as for conventional GC-MS analysis. Isotopic compositions are reported in the δ notation relative to the VPDB standard.

Major- and trace-element concentrations were determined on whole-rock samples using a wavelength-dispersive Rigaku 3040 X-ray fluorescence (XRF) spectrometer at the University of Cincinnati. Raw intensities were calibrated using a set of 65 standards from the USGS, the National Bureau of Standards, and internal lab standards that were analyzed by XRAL Incorporated using XRF and INAA. Analytical precision based on replicate analyses was better than ±2 % for major and minor elements and ±5 % for trace elements, and detection limits were 1 to 2 ppm for most trace elements.

For organic geochemical analyses, samples were extracted using dichloromethane in a Dionex ASE 200 accelerated solvent extractor (temperature: 75 °C; pressure: 50 bar). After separation of asphaltenes, the hexane soluble fractions were separated into NSO compounds, saturated hydrocarbons and aromatic hydrocarbons using medium pressure liquid chromatography with a Köhnen-Willsch instrument (Radke et al., 1980). The saturated and aromatic hydrocarbon fractions were analysed with a GC equipped with a 30 m DB-1 fused-silica capillary column (i.d. 0.25 mm; 0.25 µm film thickness) coupled to a Finnigan MAT GCQ ion trap mass spectrometer. The oven temperature was programmed from 70 to 300 °C at 4 °C/min, followed by an isothermal period of 15 min. Helium was used as carrier gas. The spectrometer was operated in the electron ionization mode over a scan range from m/z 50 to 650. Relative percentages and absolute concentrations of different compound groups in the saturated and aromatic hydrocarbon fractions were calculated using peak areas in the total ion current chromatograms in relation to those of internal standards (deuterated n-tetracosane and 1,1´-binaphthyl, resp.), or by integration of peak areas in appropriate mass chromatograms using response factors to correct for the intensities of the fragment ion used for quantification of the total ion abundance. The concentrations were normalized to TOC.

# 4. Results

## *4.1 Lithology, microfacies, and mineralogy*

At the base of the studied section, massive and thick-bedded grey limestones of the *Scheibelberg Fm.* (0.50-4.50 m; Fig. 2) are exposed. These rocks are hemipelagic to pelagic, bioturbated wackestones containing radiolarians, echinoderms, foraminifera, and ostracods. The top is formed by a breccia horizon containing carbonate lithoclasts.

The *Sachrang Member* (4.50-29.45 m; Fig. 2) comprises a 25-cm-thick basal mudstone (4.50-4.75 m), the Bächental bituminous marls (4.75-21.55 m and 22.55-29.45 m) and a debrite (21.55-22.55 m). The carbonate-free basal mudstone consists of black OM-enriched layers that are frequently interrupted by continental-derived OM-free lithoclasts. Quartz and smectite are the main minerals, whereas illite, chlorite, and plagioclase occur in minor amounts. The Bächental bituminous marls can be subdivided based on differing colour reflecting variations in OM richness. The lower part of the section (subsequently Unit 1: 4.75-11.00 m) and its upper part (Unit 3: 22.55-29.45 m) consist of greyish marls, whereas the OM-rich middle part is black-coloured (Unit 2: 11.00-21.55 m). Rocks of Units 1 and 3 are laminated to bioturbated wackestones containing mainly radiolarians and subordinated filaments (*Bositra*), ostracods, sponge spicules, and some foraminifera (Figs. 2.A, 2.E). Samples from Unit 2 show varying microfacies. In the lower part (Subunit 2a: 11.00-19.35 m) finely laminated mudstones with mainly radiolarians and additionally *Bositra*, sponge spicules, ostracods, and foraminifera occur (Fig. 2.B). Small channels, onlap structures as well as low energetic, fine-grained turbidites with carbonate detritus are present. The occasional occurrence of radiolarian wackestones in the middle and upper parts of Subunit 2a indicate episodic blooms of radiolarians as well as a significant contribution of these organisms to the planktonic biomass of the sediment (Fig. 2.C; cf. Sabatino et al., 2009). The most striking characteristic in Subunit 2b (19.35-21.55 m) is the presence of re-deposited carbonate detritus layers containing abundant pyrite (Fig. 2.D). These layers become thicker and more frequent towards the top of Unit 2, which is formed by a 1-m-thick bioturbated wackestone with reworked carbonate intraclasts, interpreted as debris flow deposit. Bioturbation is generally weak, except for samples at the base of Unit 3.

Apart from OM, the Bächental bituminous marls consist mainly of quartz and carbonate minerals. The latter appear as [i] detrital calcite, [ii] secondary calcite, and [iii] typically Mn-rich diagenetic carbonate phases (subsequently referred to as diagenetic Mn-rich carbonates) featuring varying incorporation of Mn, Ca, Mg, and Fe. Pyrite is abundant in all samples. The rock matrix consists of clay and carbonate minerals; muscovite and feldspar occur in subordinate amounts. Diagenetic Mn-rich carbonates are the most abundant carbonate minerals in the majority of samples from Units 1 and 3 showing significant vertical

variations in peak area from 2200 to 21300 (Fig. 3.A; Table 1 in the Appendix). In contrast, diagenetic Mn-rich carbonates are generally rare in Unit 2 (260-7800 in peak area; Fig. 3.A; Table 1 in the Appendix), which contains larger amounts of secondary calcite instead. Diagenetic Mn-rich carbonates appear with broad, irregular peaks in the diffractograms, suggesting a low degree of crystallinity.

The *Upper Allgäu Fm.* (30.85-35.54 m) at the top of the section is formed by an alternating sequence of bioturbated light grey limestones and dark grey marls. Both contain radiolarians, *Bositra*, and some ostracods. The contact of the *Sachrang Member* and the overlying *Upper Allgäu Fm.* is not exposed (29.45-30.85 m).

### *4.2 Bulk geochemical parameters*

The vertical variation of bulk geochemical parameters is shown in Figs. 3.B-E and 4.A. The full dataset is presented in the Appendix (Table 1). $T_{max}$ (416-427 °C) and PI values (<0.1) indicate that the bituminous marls are thermally immature. Higher $T_{max}$ values (~ 444 °C) are restricted to the basal mudstone. Limestones and marls from the *Scheibelberg Fm.* and the *Upper Allgäu Fm.* show very low TOC contents (<0.2 and 0.4%, resp.).

The basal mudstone of the *Sachrang Member* contains very low S contents (ca. 0.1%), but significant amounts of OM (TOC: 1.8%). Low HI values (74 and 37 mg HC/g TOC) indicate a high proportion of inert OM. Unit 1 of the Bächental bituminous marls is characterized by moderate TOC (1.1-3.3%) and high S contents (2.2-5.7%). $Cc_{eq}$ range between 24.4 and 43.6%. HI varies between 306 and 612 mg HC/g TOC. Fe contents are rather uniform (3.3-5.2%), but reach 9.2% in a sample at 6.65 m. Samples from Subunit 2a show a wide variety of TOC contents (2.9-12.9%). Two positive TOC excursions are visible from 11.00 to 15.65 m and from 18.05 to 19.55 m. Despite strong TOC variations, HI values are quite uniform (588-687 mg HC/g TOC). The S curve does not mirror the TOC trend but stays constant at relatively low levels (2.1-3.2%). Between 15.15 and 18.05 m S contents show strong fluctuations (1.3-7.1%) and an inverse correlation with both TOC and $Cc_{eq}$ (17.4-58.8%). Marls in Subunit 2b (18.6-38.8% $Cc_{eq}$) exhibit TOC contents from 2.9 to 6.3% and high HI values (572-683 mg HC/g TOC) and S contents (3.5-5.9%). Fe concentrations in Unit 2 vary strongly from 0.1 to 6.1%. The carbonate debrite, poor in OM and S, marks a significant change in bulk source-rock parameters. TOC contents in Unit 3 are rather uniform (~1.5-2.0%) and are slightly higher (up to 3.0%) only near its top. $Cc_{eq}$ (22.8-64.8%) and S contents (1.3-5.8%) show significant vertical variations. In general, $Cc_{eq}$ is decreasing towards the top, whereas S contents are higher in the upper half of Unit 3. HI values in the lower part

of Unit 3 are significantly lower (300-400 mg HC/g TOC) than in the underlying Unit 2 (>600 mg HC/g TOC), but show an upward increase (up to 550 mg HC/g TOC). Fe contents are rather uniform (3.2-6.1%). A single sample with only 1.4% Fe occurs at 27.55 m.

### *4.3 Organic petrology*

The basal mudstone contains mainly amorphous OM. High reflectivity suggests the presence of charred land-plant material. In addition, inertinite occurs together with traces of liptinite. The OM of the Bächental bituminous marls is dominated by lamalginite (Figs. 5.A-D). Telalginite, sporinite and fish remains are present with slightly varying, but always low amounts (Figs. 5.A-D). The sporinite content is slightly increasing upsection. Terrestrial inertinite and vitrinite occur rarely with tiny irregularly shaped particles. Consequently vitrinite reflectance could not be measured. Pyrite is frequent in Units 1 and 3, whereas most rocks of Unit 2 contain lower pyrite percentages. Pyrite appears disseminated with crystals of framboidal as well as subhedral to euhedral shape; pyritization of organism fragments (especially radiolarians) is also common. In Subunit 2b the bulk of pyrite present is bound to carbonate turbidite layers.

### *4.4. Stable isotope composition of carbonate minerals and organic matter*

Bulk carbonate and organic carbon isotope values are shown in Figs. 4.B-D. The full dataset is presented in the Appendix (Table 1). Limestones and marls from the *Scheibelberg Fm.* and the *Upper Allgäu Fm.* show rather constant $\delta^{13}C_{carb}$ isotope values (0.8 to 1.5‰ VPDB and -0.8 to 0.2‰ VPDB). The same is true for $\delta^{18}O_{carb}$ isotope values for limestone samples from the *Scheibelberg Fm.* (-2.3 to -1.2‰ VPDB) and the *Upper Allgäu Fm.* (-2.1 to -1.8‰ VPDB). In contrast, marls from the *Upper Allgäu Fm.* show significant lower $\delta^{18}O_{carb}$ isotope values (-5.0 to -3.5‰ VPDB). Isotope data from the *Sachrang Member* are more inhomogeneous. $\delta^{13}C_{carb}$ isotope values vary strongly in Unit 1 (-10.0 to -1.8‰ VPDB). In contrast, $\delta^{13}C_{carb}$ isotopes are rather constant in Unit 2 (-4.2 to -1.5‰ VPDB). While bulk carbonate isotope values of the debrite ($\delta^{13}C_{carb}$: -0.2 to 0.8‰ VPDB; $\delta^{18}O_{carb}$: -2.3 to -1.4‰ VPDB) are in the range of the *Scheibelberg Fm.*, $\delta^{13}C_{carb}$ isotopes from Unit 3 demonstrate a wide range (-12.7 to -2.2‰ VPDB). $\delta^{18}O_{carb}$ isotope values of the bituminous marls vary from -6.0 to -2.1‰ VPDB.

Organic carbon isotope values of the OM-poor *Scheibelberg Fm.* and *Upper Allgäu Fm.* are in a similar range (-28.7 to -23.6‰ VPDB and -29.4 to -25.6‰ VPDB). $\delta^{13}C_{org}$ isotope values oscillate in a narrow range in the bituminous marls (-32.7 to -30.6‰ VPDB)

and the debrite (-30.1 to -28.7‰ VPDB), showing the strongest fluctuations in Unit 2. Carbon isotope compositions of pristane (Pr) and phytane (Ph) are in a similar range (Pr: -34.6 to -33.0‰ VPDB; Ph: -34.4 to -33.1‰ VPDB) for all samples.

### *4.5 Molecular composition of hydrocarbons*

The samples show relative uniform *n*-alkane distributions characterized by high relative proportions of short- and mid-chain *n*-alkanes (*n*-$C_{15-19}$/Σ*n*-alkanes: 0.23-0.56; *n*-$C_{21-25}$/Σ*n*-alkanes: 0.26-0.43, resp.; Figs. 6, 7.A). Short-chain *n*-alkanes dominate over mid-chain *n*-alkanes in all but five samples. Long-chain *n*-alkanes (*n*-$C_{27-31}$/Σ*n*-alkanes) are present with proportions from 0.05 to 0.32 (Figs. 6, 7.A). The carbon preference index (CPI; after Bray and Evans, 1961) varies between 0.85 and 3.20 with lowest values in Unit 2. The vertical variation of the acyclic isoprenoid ratio (Pr/Ph) is shown in Fig. 7.B. The Pr/Ph ratio is moderately high in Units 1 and 3 (0.88-1.76) and generally lower in Subunits 2a (0.70-1.01) and 2b (0.89-1.30).

Among steroids, the ααα-steranes are present in the range of $C_{27}$ to $C_{29}$ and predominate over βαα-isomers (Fig. 8). The ratio of $C_{27}$ vs. $C_{29}$ steranes (Fig. 7.C) increases upwards from 0.70 to 1.24 in the lower part of Unit 1 and decreases in the upper part. The ratio is very low (~0.60) in the lowermost 3 m of Subunit 2a and increases upwards to reach a maximum of 1.10 in Subunit 2b. In Unit 3 the ratio varies from 0.59 to 1.03. The ratio of $C_{27}$/$C_{29}$ αααR steranes displays a similar vertical trend (Fig. 7.C). Diasteranes occur with low concentrations and are represented by their $C_{27}$ homologues in all units. $C_{29}$ diasteranes are restricted to Unit 1. The ratio of 4-methylsteranes vs. Σ$C_{29}$ steranes is relatively high in the lower part of the section and decreases sharply from 3.10 to 1.04 at the boundary between Subunits 2a and 2b (Fig. 7.D). The ratio of 20*S*/(20*S* + 20*R*) isomers calculated from ααα $C_{29}$ steranes is generally between 0.11 and 0.18 in Units 1, 2b and 3 (Fig. 7.E). Two outliers occur at 6.15 m (0.27) and 22.60 m (0.32). The ratio in Subunit 2a is higher (0.25-0.33). The vertical trend of mono- vs. triaromatic steroids is shown in Fig. 7.D. It displays a reversed image to the sterane isomerization ratio, with low values for Unit 2 (1.25-2.17) and high ratios for the rest of the succession (up to 3.81).

The hopane distribution is characterized by the predominance of αβ homologues from $C_{27}$ to $C_{35}$; additionally βα hopanes and bisnorhopane could be detected (Fig. 9). Bisnorhopane is enriched in Subunit 2a (25.7-124.7 µg/g TOC) compared to the remaining units (2.5-56.3 µg/g TOC). The ratio of 22*S*/(22*S* + 22*R*) isomers of the αβ $C_{31}$ hopane varies from 0.39 to 0.64 (Fig 7.F). The vertical trend with high values in Subunit 2a (0.50-0.64; Fig.

7.F) is identical to the sterane isomerization. Gammacerane could be detected in all samples. The gammacerane index [GI = gammacerane/(gammacerane + αβ $C_{30}$ hopane)] reaches maximum values (0.80) in Subunit 2a and is lower in the other units (0.05-0.59; Fig. 7.F).

Aryl isoprenoids occur in all samples, but their concentrations vary significantly (3.2-112.1 µg/g TOC). The median values of different units suggest a general upward increase from ca. 15 µg/g TOC (Units 1, 2a) to values exceeding 50 µg/g TOC (Units 2b, 3). Dibenzothiophene (DBT) and phenantrenes (Phen) are present with variable amounts in all samples. The DBT/Phen ratio is low in Units 1 and 3 (0.23-0.48) and higher in Subunits 2a (0.64-0.83) and 2b (0.46-0.60; Fig. 7.E). The full dataset of organic geochemical analyses is presented in the Appendix (Tables 2, 3).

# 5. Discussion

## *5.1 Organic matter sources and preservation*

### *5.1.1 Thermal Maturity*

The degree of thermal maturity can be estimated using vitrinite reflectance (VR), Rock Eval parameters ($T_{max}$, PI), and biomarker ratios. However, some biomarker ratios can be inaccurate as maturity indices when applied to the study units. The measurement of VR was impossible because of the low amount and small size of vitrinite particles in the study samples. Low thermal maturity is indicated by low $T_{max}$ and PI values. The equation VR = 0.018 x $T_{max}$ – 7.16, proposed for type I and II kerogen (Peters et al., 2005) suggests a maturity corresponding to a VR of ca. 0.45% $R_o$. The occurrence of charred organic material in the basal mudstone suggest that its elevated $T_{max}$ values, corresponding to a VR of ca. 0.80% $R_o$ (equation after Peters et al., 2005), are due to the change in organic matter type.

Isomerization ratios of hopanes and steranes in samples from Units 1, 2b, and 3 as well as aromatization of steroids are consistent with a maturity in the range of 0.40 to 0.50% $R_o$ (cf. Mackenzie and Maxwell, 1981; Mackenzie et al., 1982). However, biomarker ratios suggest a slightly higher thermal maturity (~0.60% $R_o$) for Subunit 2a, which is located in the middle part of an undisturbed and continuous succession. A thermal overprint as the reason for the apparent higher maturity can be excluded. Salinity and/or lithotype variations are regarded as possible triggers of sterane ratio variations (ten Haven et al., 1986; Peters et al., 1990). Bitumen from immature source rocks deposited under hypersaline conditions tends to show more mature hopane patterns owing to unusual diagenetic pathways (ten Haven et al., 1987). For this reason, isomerization ratios are not reliable as a maturity parameter in Subunit

2a (see section 5.2.2), and the Bächental bituminous marls are inferred to have a low maturity corresponding to a VR of 0.40 to 0.50% $R_o$. These results confirm the questionability of applying isomerization ratios as maturity proxies to sections deposited under hypersaline conditions or strongly variable salinities.

*5.1.2 Organic matter sources*

The relative proportions of marine and terrestrial OM determine the kerogen type and provide information about OM source, productivity, and preservation, as well as basin setting and water depth. OM of the basal mudstone mainly consists of charred material indicating terrestrial sources. The occurrence of charred OM is commonly connected to wildfire activity (e.g., Brown et al., 2012). In contrast, the dominant maceral group in Bächental bituminous marls is alginite, which suggests a mainly marine algal source of OM (Taylor et al., 1998). The most abundant maceral is lamalginite, which may derive from thin-walled planktonic and benthic organisms, including green algae, cyanobacteria, and bacterial mats (Oschmann, 2000). Telalginite originates from algae such as *Botryococcus*, *Tasmanites*, and *Gloeocapsomorpha* that occur as thick-walled unicellular organisms with some internal structure (Hutton, 1987). The low frequency of vitrinite and inertinite suggests terrestrial inputs of OM to be of subordinate importance. The occurrence of radiolarian wackestones in the middle and upper part of Subunit 2a indicates episodic blooms of radiolarians and, hence, significant input of OM from planktonic heterotrophs as well as autotrophs.

HI values vary considerably within the study section, suggesting a mixture of kerogen types II and III. However, relatively invariant maceral compositions imply that OM is derived dominantly from marine algae and bacterioplankton, an inference also supported by the predominance of low molecular weight *n*-alkanes (<*n*-$C_{20}$; Cranwell, 1977). Variations in HI values therefore reflect an early diagenetic overprint rather than multiple OM sources (see section 5.1.3). Unit 2 has been less affected by this diagenetic overprint than Units 1 and 3, and its HI of 600 to 700 mg HC/g TOC, which is indicative of type II kerogen, is taken as representative of primary OM in the entire section. The primary (i.e., pre-diagenetic) HI of diagenetically altered OM can be estimated from a plot of TOC vs. $S_2$ (Langford and Blanc-Valleron, 1990), which yields values of ~770 mg HC/g TOC for Units 1 and 3 of the study section (correlation coefficient $r^2 = 0.99$). This is consistent with little variation in kerogen type through the entire profile and a dominantly marine source of OM. The varying HI values are therefore not reflecting the primary source of OM but are rather caused by the mineral

matrix effect (Langford and Blanc-Valleron, 1990). However, an influence of early diagenetic OM oxidation on reduced HI values is also likely (cf. Röhl et al., 2001).

Biomarkers provide additional insights regarding OM sources. Algae are the predominant producers of $C_{27}$ sterols; $C_{29}$ sterols are more typically associated with land plants (Volkman and Maxwell, 1986). However, results from biomarker studies add to the growing list of microalgae that contain high amounts of 24-ethylcholesterol (Volkman et al., 1999; Peters et al., 2005). 4-methylsteroids with a $C_{30}$ dinosterol structure are considered as biomarkers of dinoflagellates (Robinson et al., 1984), while others are related to marine and lacustrine precursors (Mackenzie et al., 1982; Volkman et al., 1990; Peters et al., 2005; Auras and Püttmann, 2004). Thus, the relative abundance of non-aromatic steroids in the Bächental bituminous marls indicate the contribution of biomass from marine phytoplankton and a minor input of terrestrial OM. The 4-methylsteranes most probably originate from dinoflagellates (see also Köster et al., 1995). The most probable biological precursors of the hopane derivatives found in the samples are bacteriohopanepolyols (Ourrison et al., 1979; Rohmer et al., 1992). These compounds have been identified in bacteria as well as in some cryptogames (e.g., mosses and ferns) and in sulphate-reducing bacteria (Blumenberg et al., 2006). The predominance of homohopanes up to $C_{35}$ and the occurrence of benzohopanes from $C_{22}$ to $C_{35}$ in the aromatic hydrocarbon fraction suggest that bacteriohopaneols were a significant constituent of the biomass. In summary, we infer that algal and bacterial biomass of marine origin are the predominant OM sources for Bächental bituminous marls whereas OM input from terrestrial sources is of minor importance. In contrast, the bulk of OM contained in the basal mudstone, including charred material, was derived from terrestrial sources.

*5.1.3 Influence on organic matter by diagenetic processes*

Varying environmental conditions in the Bächental basin also affected diagenetic processes. Different degrees of bacterial degradation of OM and concurrent formation of diagenetic Mn-rich carbonates had a significant impact on bulk source-rock parameters. Early diagenetic degradation mainly controlled OM preservation in Units 1 and 3. This is supported by low TOC contents and HI values, which show a correlation with the amount of diagenetic Mn-rich carbonates. In Units 1 and 3, labile algal OM primarily present in the samples was degraded to a rather constant residual TOC level of ca. 2% during early diagenesis. The generated $^{12}C$-enriched carbon was fixed in diagenetic Mn-rich carbonates.

The carbonate C-isotope profile of the study section has been strongly influenced by these diagenetic processes, resulting in a mixed signal derived from primary and secondary carbonate phases. The vertical trends of $\delta^{13}C_{carb}$ isotope values and diagenetic Mn-rich carbonate contents show a significant negative correlation (compare Figs. 3.A and 4.B). Isotope ratios get more negative with increasing amounts of diagenetic Mn-rich carbonates, especially where high contents are observed in Units 1 and 3. The carbonate C-isotope compositions of the diagenetic Mn-rich carbonates in those units were determined by the relative proportions of isotopically light carbon from early diagenetic degradation of OM on the one hand and isotopically heavy seawater-sourced dissolved inorganic carbon in sediment pore waters on the other. A minor input of organic-derived carbon into calcite is also possible but not important compared to the strength of the effect on diagenetic Mn-rich carbonates. Very low $\delta^{13}C_{carb}$ values (-11‰ VPDB) in limestone beds of the Posidonia Shale are also attributed to early diagenetic carbonate precipitation and incorporation of $^{12}C$-rich carbon derived from organic matter degradation via sulphate reduction (Röhl et al., 2001).

Unit 2 exhibits anomalously heavy $\delta^{13}C_{carb}$ values (-2 to -3‰ VPDB) compared to Units 1 and 3, but values that are nonetheless lighter than those of other lower Toarcian sections (~0‰ VPDB; e.g. Röhl et al., 2001; Hesselbo et al., 2007; Sabatino et al., 2009). These relatively heavy $\delta^{13}C_{carb}$ values are interpreted to be least altered (i.e., relative to primary marine carbonate phases). In Unit 2, the bulk of carbonate present is secondary calcite whereas the quantity of diagenetic Mn-rich carbonates is typically low (Fig. 3.A). The lack of the latter also implies smaller amounts of organically sourced carbon that were fixed in secondary carbonates of Unit 2. The precipitation of diagenetic Mn-rich carbonates was inhibited because anoxic bottom waters existed during deposition of Unit 2 (cf. Calvert and Pedersen, 1996; see Section 5.2.1). Overall, it is clear that the measured $\delta^{13}C_{carb}$ values reflect the nature and extent of diagenetic processes rather than the primary isotopic signal.

The carbonate O-isotope composition of the study section is also dominated by diagenetic effects. The heaviest values (~-1.0‰ VPDB) are found in the limestones underlying the Bächental bituminous marls (Fig. 4.C). These values are consistent with a primary normal-marine isotopic composition (~-1.0‰ VPDB, ice-free; e.g., Röhl et al., 2001). All $\delta^{18}O_{carb}$ isotope ratios for the bituminous marls record shifts toward lighter isotopic compositions that are a function of precipitation of diagenetic carbonate at burial temperatures exceeding contemporaneous sea-surface temperatures (cf. Algeo et al., 1992). The more $^{18}O$-depleted values are likely to represent precipitation of secondary phases at later diagenetic stages and, hence, higher burial temperatures (cf. Algeo et al., 1992). For this reason,

diagenetic carbonate in Units 1 and 3 appears to have formed earlier on average than that in Unit 2. This inference indicates an earlier formation of diagenetic Mn-rich carbonates in Units 1 and 3 compared to the secondary calcite of Unit 2. $\delta^{18}O_{carb}$ isotope ratios for the epicontinental Posidonia Shale of Dotternhausen plot within a narrower range (~-5.0 to -7.0‰ VPDB) compared to those of the Alpine Bächental bituminous marls (~-2.0 to -6.0‰ VPDB). However, whereas the former represents a primary depositional signal derived from carbonate of well-preserved coccoliths and schizosphaerelles (Röhl et al., 2001), the $\delta^{18}O_{carb}$ signal of the latter was controlled by diagenetic processes.

## *5.2 Depositional environmental conditions*

### *5.2.1 Redox conditions and iron availability*

The Latest Triassic and the Early Jurassic were characterized by global perturbations caused by the activity of LIPs (CAMP, Karoo-Ferrar; Marzoli et al., 1999; Svensen et al., 2007, 2013; Jourdan et al., 2008; Caruthers et al., 2013; Sell et al., 2014) and the rifting of the Alpine Tethys in the Penninic realm with oceanic break-up in the Pliensbachian/Toarcian (Ratschbacher et al., 2004; Mohn et al., 2010; Decarlis et al., 2013) that induced major environmental changes and climate warming ("greenhouse Earth" conditions; Palfy and Smith, 2000; Weissert, 2000; Jenkyns, 2003) resulting in oceanic conditions generally conducive to development of anoxia. The prevailing redox conditions in a depositional basin commonly vary with time and are sensitive to changes in environmental conditions as reflected in the stratigraphic trends of various proxies (e.g., Pr/Ph ratio, arylisoprenoids, bioturbation, and Fe-TOC-S) in the sedimentological record.

In the study section, extensive bioturbation and relatively low TOC contents are indicative of normal-marine conditions without major perturbations of the carbon cycle during deposition of the *Scheibelberg Fm.* and the *Upper Allgäu Fm.* In contrast, redox conditions varied significantly during deposition of the Bächental bituminous marls, as shown by the multiple redox proxies discussed below.

The Pr/Ph ratio is commonly used as a redox indicator during early diagenesis. According to Didyk et al. (1978), Pr/Ph ratios <1.0 indicate anaerobic conditions whereas values >1.0 speak for suboxic to oxic environments. However, Pr/Ph ratios are also known to be affected by maturation (Tissot and Welte, 1984) and different precursors for isoprenoids (Goosens et al., 1984; Volkman and Maxwell, 1986; ten Haven et al., 1987). Both influences can be ruled out in the case of the Bächental section, because of its limited thickness and the similar isotopic compositions of Pr and Ph, which indicates a common precursor. Hence,

Pr/Ph ratios suggest generally suboxic conditions for Units 1 and 3; however, short-term anoxia cannot be completely excluded. In contrast, an environment with strictly anoxic bottom waters is suggested for Subunit 2a. Subunit 2b features a shift to less reducing (i.e. suboxic to anoxic) conditions. The postulated paleoredox trend is also visible in a plot of Pr/Ph vs. DBT/Phen (Fig. 10). The vertical redox trend suggested by Pr/Ph ratios is confirmed by bioturbation patterns. Small-scale bioturbation is visible in sections from Units 1 and 3, but totally missing in Unit 2. In addition, the occurrence of larger amounts of bisnorhopane argues for an elevated input of anaerobic bacteria typical of predominantly anoxic conditions in Unit 2 (Grantham et al., 1983; Rullkötter and Wendisch, 1982; Watson et al., 2009). Aryl isoprenoids derive from special green sulphur bacteria (Chlorobiaceae) that perform anoxygenic photosynthesis which requires light penetration into $H_2S$ saturated waters (Schwark and Frimmel, 2004). Therefore, aryl isoprenoids can be used to estimate whether the anoxic water column extended into the photic zone (Summons and Powell, 1986; Grice et al., 1996a; Koopmans et al., 1996). Aryl isoprenoids occur in all samples, although in variable amounts, suggesting frequent but transient episodes of photic-zone anoxia.

Several authors used TOC/S ratios for determining paleoredox conditions (e.g. Berner, 1970, 1984; Leventhal, 1983; Berner and Raiswell, 1983). However, this approach is problematic when Fe is limiting, as is often observed in carbonate environments (cf. Berner and Raiswell, 1983; Raiswell and Berner, 1985). The ternary plot of Dean and Arthur (1989) additionally includes Fe contents and consequently all phases relevant for pyrite formation. Therefore, this approach is used for the Bächental section. Most samples of Units 1 and 3 plot either along the pyrite line or in the field of excess Fe availability (Fig. 11). The former indicates anoxic conditions and a sulfidization of all the available Fe; the latter suggests the presence of non-pyritized Fe and suboxic conditions during deposition (Dean and Arthur, 1989; Hofmann et al., 2000; Rimmer et al., 2004). Hence, varying suboxic and anoxic conditions with intense sulphate reduction rates are reflected by the Fe-TOC-S diagram for Unit 1 and the upper part of Unit 3, whereas less reducing conditions prevailed during deposition of the lower part of Unit 3. The large amounts of available Fe in Units 1 and 3 triggered enhanced pyritization during diagenesis. In contrast, the Fe-TOC-S diagram confirms Fe limitation in TOC-rich samples of Unit 2 (Fig. 11) consistent with a postulated anoxic to euxinic environment. The presence of excess S in Subunit 2a is reflected by elevated DBT/Phen ratios due to the incorporation of S in the aromatic fraction of OM during early diagenesis (“natural sulphurization”; Kohnen et al., 1991).

The negative correlation of S contents with both TOC and $Cc_{eq}$ in the interval from 15.15 to 18.05 m (Subunit 2a; Figs. 3.B-D) suggests changing Fe availability and alkalinity. The large amounts of $H_2S$ produced in the OM-rich layers by sulphate reduction could not be fixed as pyrite because of an insufficient amount of reactive Fe, resulting in significant amounts of free $H_2S$. Only a small portion of this $H_2S$ was incorporated in OM, producing elevated DBT/Phen ratios in the high-TOC/low-S layers, whereas the excess free $H_2S$ diffused upward until it was fixed as pyrite in layers with relatively low TOC contents but large amounts of reactive Fe, resulting in low-TOC/high-S intervals (cf. Jaminski et al., 1998). The high alkalinity generated by sulphate reduction (e.g., Thomas et al., 2008) triggered the enhanced precipitation of secondary calcite in the high-TOC/low-S intervals. Iron-limiting conditions are directly connected to the available pool of Fe oxides (Raiswell et al., 1994). Several studies confirm a direct relationship between bulk sedimentation rates and variable organic input and clastic flux, respectively (cf. Mangini and Dominik, 1979; Kuehl et al., 1993; Arthur et al., 1994; Jaminski et al., 1998). The mudstone samples of Subunit 2a were deposited in a low-energy environment characterized by the rareness of detrital carbonate layers. We interpret the absence of turbiditic input to have caused Fe limitation in those samples. In contrast, infrequent carbonate turbidites within Subunit 2b provided sufficient reactive Fe to fix $H_2S$ as pyrite in an otherwise Fe-limited environment (e.g., Fig. 2.D). Consequently, the bulk of pyrite present in Subunit 2b is bound to fine-grained carbonate turbidites. Therefore, detrital influx controlled Fe availability and the degree of pyritization in Unit 2.

Summing up, several redox changes affected the depositional environment of the Bächental bituminous marls. Suboxic to possibly short-term anoxic conditions prevailed during deposition of Units 1 and 3. Intense sulphate reduction and oxidation of OM in the sediment during diagenesis generated $H_2S$ that reacted with available Fe in the basin to produce large amounts of pyrite in Units 1 and 3. In contrast, all redox parameters suggest anoxia for Unit 2. Strongly reducing Subunit 2a is Fe-limited in large part, whereas carbonate turbidites triggered pyritization and, in addition, induced a shift to less reducing (i.e. suboxic to anoxic) conditions during deposition of Subunit 2b.

*5.2.2 Salinity and water-column stratification*

Several authors suggested salinity stratification caused by basin restriction resulting from minor sea-level fluctuations to be the trigger of black shale deposition in the European Toarcian (e.g. Röhl et al., 2001; Frimmel et al., 2004; van de Schootbrugge et al., 2005).

Salinity stratification may have resulted from an accelerated hydrological cycle due to a monsoonal climate reducing the salinity of ocean-surface waters (e.g., Sælen et al., 1996). The reconstruction of salinity changes during deposition of the Bächental bituminous marls is based on GI and a plot of GI vs. 4-methylsteranes/$\Sigma C_{29}$ steranes (Fig. 12). High values for GI indicate a stratified water column in marine and non-marine source-rock depositional environments, commonly resulting from a deep hypersaline water body (Fu et al., 1986). Alternatively, gammacerane may also originate from bacterivorous ciliates floating at the chemocline within the water column (Sinninghe Damsté et al., 1996; Schwark et al., 1998). According to these studies, elevated amounts of gammacerane might reflect a well-stratified water column, even in the absence of high-salinity bottom waters. However, the occurrence of bottom waters with elevated salinity in the Bächental basin is also confirmed by increased hopane isomerization ratios, which result from diagenetic processes specific for hypersaline conditions (ten Haven et al., 1987; see also section 5.1.1), as well as by large amounts of 4-methylsteranes, which are frequently related to halophilic microorganisms (e.g., ten Haven et al., 1985). A well-defined positive correlation exists between GI and 4-methylsteranes (Fig. 12). The profiles of both GI and 4-methylsteranes indicate normal-marine salinity conditions during deposition of Units 1, 2b and 3. In contrast, generally enhanced salinity of bottom waters and a stratified water column is suggested for samples from Subunit 2a.

During deposition of Unit 1, frequent mixing and ventilation of the water column of the Bächental basin prevented the establishment of a stratified water mass and permanent anoxic conditions. The transition to OM-rich Subunit 2a was associated with a distinct increase of bottom water salinity and a concomitant flourishing of halophilic microorganisms. This interval is assigned to the lower *falciferum* Zone on the basis of occurrences of *Cleviceras exaratum*. Samples of Subunit 2a are also characterized by Pr/Ph ratios <1.0. Hence anoxic conditions in Subunit 2a were typically connected to a stratified water column. Elevated inputs of freshwater due to an accelerated hydrological cycle resulted in a surface-water layer with reduced salinity that caused intensified water-column stratification (Praus and Riegel, 1989; Littke et al., 1991; Sælen et al., 1996) and also may have contributed to salinity variation within the Bächental basin. Transient small-scale mixing of the watermass caused by turbidites triggered an episodic decrease of bottom water salinity reflected by lower GI values for a few samples from the middle and upper parts of Subunit 2a (e.g., 15.65 and 16.55 m; Figs. 7.F, 12). Those samples are additionally characterized by comparatively low TOC and peak S contents (Figs. 3.B, D). Whereas a stagnant basin setting prevailed during deposition of Subunit 2a, the episodic occurrence of fine-grained carbonate turbidites caused

644 salinity stratification to break down, resulting in less intensely reducing conditions in Subunit
645 2b (see Section 5.2.1). During deposition of Unit 3 a water column with uniform normal
646 salinity went along with suboxic conditions. The observed salinity variations suggest that
647 global climate processes as described for instance by Sælen et al. (1996) were overprinted by
648 local factors within the Bächental basin, e.g., mixing of water bodies by turbidites, which also
649 influenced the intensity of water-column anoxia.
650
651 *5.2.3 Influence of sea-level variation*
652 Variation in sea-level elevations exerted a pronounced influence on deposition of both
653 the Alpine Bächental bituminous marls and the epicontinental Posidonia Shale (e.g., Röhl et
654 al., 2001; Frimmel et al., 2004). The long-term eustatic record shows a sea-level fall from the
655 Pliensbachian into the early Toarcian, a subsequent sea-level rise culminating in a middle
656 Toarcian highstand, and another fall extending into the Aalenian (Haq et al., 1988; Hallam,
657 1992). However, the short-term trend exhibits several additional sea-level fluctuations in
658 Pliensbachian and Toarcian time (Fig. 13). Frimmel et al. (2004) found a remarkable
659 correlation between the trend of $C_{27}/C_{29}$ sterane ratios and the proposed sea-level trend of Haq
660 et al. (1988) for the Posidonia Shale of Dotternhausen. Although sea-level estimations based
661 on biomarker ratios are a rather untested technique, the sterane data for the Alpine Bächental
662 bituminous marls also show a strong correlation with the 3$^{rd}$ order sea-level curve for the
663 upper Pliensbachian-lower Toarcian interval (Haq et al., 1988; Fig. 13). These similar
664 relationships thus provide a basis for correlation of the Bächental bituminous marls with the
665 Dotternhausen section (Fig. 13; Frimmel et al., 2004; see Section 5.3.1). According to sterane
666 ratios of the study section, the sea-level rise from the base of Unit 1 reached a highstand
667 around 9 m, followed by an abrupt sea-level fall. The deposition of Subunit 2a, recording the
668 highest TOC contents, coincided with a sea-level lowstand dated to the lower *falciferum* Zone
669 based on the occurrence of *Cleviceras exaratum*, and a subsequent minor sea-level rise.
670 Another highstand was reached close to the debrite overlying Subunit 2b, followed by minor
671 sea-level fluctuations during deposition of Unit 3.
672 Sea-level fluctuations strongly influenced watermass exchange and hence ventilation
673 of the Bächental basin (Fig. 14). Agreement between the sea-level curve and inferred
674 variations in redox conditions and salinity demonstrate this influence. During the sea-level
675 lowstand (Subunit 2a), watermass exchange and consequently oxygenation of basinal bottom
676 waters were sharply reduced. Consequently, strongly anoxic conditions were established
677 within the stratified watermass. High surface-water productivity and subsequent degradation

of OM additionally poisoned the depositional environment. Hence, Subunit 2a is generally characterized by strongly anoxic conditions and high OM preservation reflected by high TOC and HI values. The same correlation between stagnant basin conditions, strongest anoxia and best OM preservation during a sea-level lowstand and a subsequent sea-level rise has been postulated for the epicontinental Posidonia Shale of SW Germany (e.g. Röhl et al., 2001; Schmid-Röhl et al., 2002; Frimmel et al., 2004; see Section 5.3.1). In addition, a flourishing of surface-water productivity during the uppermost *tenuicostatum* to lower *falciferum* zones (e.g., Ikeda and Hori, 2014) contributed to elevated OM accumulation in Subunit 2a (see Section 5.2.4). During intervals of higher sea level (e.g., Units 1 and 3), better watermass exchange with surrounding epicontinental seas and, possibly, the open Tethys Ocean resulted in improved ventilation of the Bächental basin and in mainly suboxic conditions, reflected by sediments with lower TOC concentrations. Therefore, we suggest that minor sea-level fluctuations in combination with the complex bathymetry of the Bächental basin were among the controlling factors on deposition of the Bächental bituminous marls (Fig. 14). Consequently, the local basin setting had a strong influence on the establishment of salinity stratification and anoxic conditions.

*5.2.4 Marine primary productivity*

Marine primary productivity is likely to have been influenced by major changes in global climate, atmospheric composition, and oceanographic conditions during the Early Jurassic. Eruption of the Karoo and Ferrar large igneous provinces (Encarnación et al., 1996; Svensen et al., 2007; Sell et al., 2014) triggered massive perturbations of the global carbon cycle, leading to strong global warming through volcanic $CO_2$ emissions (McElwain et al., 2005), possible methane release from gas hydrates (Hesselbo et al., 2000), and metamorphism of Paleozoic OM-rich shales (Svensen et al., 2007; Suan et al., 2008). The prevailing subtropical climate during the early Toarcian induced an acceleration of the hydrological cycle, modulated by astronomical forcing (Kemp et al., 2005), and an intensification of continental weathering (Palfy and Smith, 2000; Weissert, 2000; Cohen et al., 2004). These processes resulted in an elevated supply of nutrients to ocean-surface waters, stimulating marine primary productivity (Parrish and Curtis, 1982; Parrish, 1993; Cohen et al., 2004). Jenkyns (2010) hypothesized that there was a globally synchronous increase in organic productivity in the early Toarcian (upper *tenuicostatum*-lower *falciferum* zones) triggered by high levels of nutrient availability in surface waters. Orbital-scale productivity cycles are suggested to have triggered onset and termination of the T-OAE (Ikeda and Hori, 2014).

A detailed interpretation of stratigraphic variations of primary productivity is not possible for the Bächental section owing to intense bacterial degradation of OM in Units 1 and 3 (see Section 5.1.3). However, the remarkable amounts of S in those units suggest a high amount of OM originally present in rocks. Therefore, it is suggested that, on average, high primary production of OM in surface waters prevailed throughout the interval of deposition of the Bächental bituminous marls. Relatively high and uniform HI values suggest a lesser degree of OM degradation in Unit 2. For this reason, TOC variations in Unit 2 are inferred to reflect changes in surface-water primary productivity. This interval is also characterized by a significant TOC increase in the study section (Fig. 3.A) and in several age-equivalent sections in the European and Mediterranean domains (Jenkyns et al., 1988; Hesselbo et al., 2000; Röhl et al., 2001; Kemp et al., 2005; Pearce et al., 2008; Sabatino et al., 2009; Kafousia et al., 2014). The two samples that exhibit peak TOC contents after steady increases (at 13.39 m and 19.15 m) are also significantly enriched in short-chained *n*-alkanes (Fig 7.A). Hence, a flourishing of marine algae and bacterioplankton in surface waters contributed to elevated OM accumulation at least in parts of Subunit 2a.

There is an ongoing discussion whether enhanced organic productivity or increased preservation was the main controlling factor behind the accumulation of OM-rich deposits in the lower Toarcian (e.g., Demaison and Moore, 1980; Pedersen and Calvert, 1990; Ikeda and Hori, 2014). Increased bioproductivity results in larger amounts of OM in bottom sediments that subsequently can accelerate the establishment of reducing conditions due to oxygen depletion by enhanced OM degradation (e.g., Röhl et al., 2001; Ikeda and Hori, 2014). The intervals exhibiting productivity maxima in Subunit 2a are also characterized by a salinity-stratified watermass and intense anoxia during a period of relative sea-level lowstand (see Sections 5.3.1-3). Hence, it cannot be fully resolved whether increased productivity or enhanced preservation controlled OM accumulation in those units. However, as strictly reducing conditions and high-salinity bottom waters typically dominated during deposition of Subunit 2a, we suggest that the TOC cycles culminating at 13.39 m and 19.15 m reflect primary productivity cycles during periods of rather constant depositional conditions.

## ***5.3 Broader implications***

### *5.3.1 Correlation and dating of Bächental bituminous marls*

C-isotope chemostratigraphy has been widely used to correlate and date sections with poor biostratigraphic control (see Weissert, 2013 for summary). The early Toarcian is characterized by a distinct negative carbon isotope excursion (CIE) that is commonly

recorded by both marine carbonates and marine and terrestrial OM, and that has been used as a global chemostratigraphic marker (e.g., Sabatino et al., 2009; Al-Suwaidi et al., 2010; Mazzini et al., 2010; Gröcke et al., 2011; Caruthers et al., 2011; Sell et al., 2014). As discussed in Section 5.1.3, the carbonate C-isotope profile of the Bächental bituminous marls records a mixed signal derived from primary and secondary carbonate phases. The diagenetic overprint especially in Units 1 and 3 is sufficiently strong that it is not possible to extract the primary isotopic signal, and, hence, correlation with age-equivalent sections on the basis of $\delta^{13}C_{carb}$ chemostratigraphy is not possible.

An alternative for correlation of the poorly dated Bächental bituminous marls with the biostratigraphically well-dated epicontinental German Posidonia Shale is provided by sterane ratio profiles. The Posidonia Shale includes three ammonite biozones (from base to top): *tenuicostatum*, *falciferum*, and *bifrons* (Riegraf et al., 1984, 1985; see also Röhl et al., 2001; Frimmel et al., 2004). Frimmel et al. (2004) documented systematic stratigraphic variation in sterane ratios ($C_{27}/C_{29}$; $C_{27}/C_{29}$ ααα*R*) at Dotternhausen in SW Germany. The onset of Posidonia Shale deposition is characterized by a shift to lower ratios, from 1.0 in the underlying strata to 0.6 to 0.8 in the lower *tenuicostatum* Zone (Fig. 13). Sterane ratios increase progressively through the *falciferum* Zone and peak at ~1.4 in the lowermost *bifrons* Zone before declining abruptly to constant values of 0.7-0.9 upsection. It has to be mentioned that stratigraphic correlation based on biomarker data is a rather untested and unconventional technique. Nevertheless, the Bächental bituminous marls exhibit an almost identical pattern of stratigraphic variation in sterane ratios, although absolute values are about 20% lower relative to the Dotternhausen section (Fig. 13). According to this correlation, accumulation of the Bächental bituminous marls in the Alpine realm commenced during Pliensbachian time (*margaritatus* Zone), which is consistent with reports of the presence of *Arieticeras* sp. and *Arieticeras* sp. or *Leptaleoceras* sp. from Unit 1 (Kodina et al., 1988). This correlation demonstrates that the base of the Bächental bituminous marls is distinctly older than the base of the Posidonia Shale deposited in epicontinental areas of SW Germany (*tenuicostatum* Zone; Riegraf et al., 1984, 1985; Frimmel, 2004). Units 2 and 3 at Bächental are correlative with the Posidonia Shale, with Subunit 2a dating to the mid-*tenuicostatum* to upper *falciferum* zones, Subunit 2b to the uppermost *falciferum* and lowermost *bifrons* zones, and Unit 3 to the *bifrons* Zone. This correlation is supported by the occurrence of *Cleviceras exaratum*, which suggests a stratigraphic age for the base of Subunit 2a (13.40 m) equivalent to the lower *falciferum* Zone, as well as by common patterns of sea-level variation in the Bächental and Dotternhausen sections (Fig. 13; see Section 5.2.3). On the basis of these considerations, we

infer that the onset of black marl deposition in the Alpine and epicontinental realm was not coeval (Fig. 13). Global forces were overprinted by local factors regarding timing of initiation of OM-accumulation in different basin settings in Pliensbachian and Toarcian times.

*5.3.2 Applicability of the lower Toarcian CIE as stratigraphic marker*

A pronounced negative CIE is widely regarded as a defining characteristic of the T-OAE and a global chemostratigraphic marker for the uppermost *tenuicostatum* and lower *falciferum* zones. This negative CIE has been reported from sections in NW Europe and the Mediterranean (e.g., Röhl et al., 2001; Jenkyns et al., 2001; Kemp et al., 2005; Hesselbo et al., 2007; Sabatino et al., 2009; Kafousia et al., 2014), the NE paleo-Pacific ocean (Caruthers et al., 2011), South America (Al-Suwaidi et al., 2010; Mazzini et al., 2010; Sell et al., 2014), and northwestern Panthalassa (Izumi et al., 2012). The negative CIE has been related to a rapid release of biogenic methane by dissociation of methane hydrates (e.g., Hesselbo et al., 2000, 2007; Jenkyns et al., 2002; Kemp et al., 2005), release of large volumes of $CO_2$ due to the emplacement of the Karoo-Ferrar LIP (e.g., Palfy and Smith, 2000; Mazzini et al., 2010), thermogenic methane resulting from the intrusion of igneous rocks into Gondwanan coals (McElwain et al., 2005; Svensen et al., 2007), recycling of OM ("recycling model"; Küspert, 1982, 1983; Röhl et al., 2001), and to the contribution of OM deriving either from calcareous or organic-walled plankton (Jenkyns and Clayton, 1986). Caruthers et al. (2011) inferred that the early Toarcian negative CIE was a global signal that had been imprinted on all active global reservoirs of the exchangeable carbon cycle. However, both the organic and inorganic carbon isotope profiles of the Bächental section do not show the typical early Toarcian negative CIE (Figs. 4.B, D).

Whereas carbonate C-isotope values of Units 1 and 3 reflect a strong diagenetic overprint, $\delta^{13}C_{carb}$ values of Unit 2 are interpreted to be less altered (see Section 5.1.3). Age correlation based on sterane data (see Section 5.3.1) as well as the occurrence of *Cleviceras exaratum* suggests an upper *tenuicostatum* to lower *falciferum* Zone assignment for the lower half of Subunit 2a, i.e., equivalent in time to the early Toarcian negative CIE. However, neither the organic $\delta^{13}C$ nor the carbonate $\delta^{13}C$ profile of the study section exhibits the early Toarcian negative CIE for reasons that remains unclear.

$\delta^{13}C_{org}$ compositions for the Bächental bituminous marls are considerably lighter (-32.7 to -30.6‰ VPDB) than typical values for modern marine plankton (-24 to -18‰ VPDB; e.g., Lewan, 1986; Tyson, 1995). They are also significantly lighter than average values of other lower Toarcian profiles as the $\delta^{13}C_{org}$ values of the entire Bächental bituminous marls

succession are in the range of the lower Toarcian negative organic CIE (Hesselbo et al., 2000; Kemp et al., 2005; Röhl et al., 2001; Sabatino et al., 2009; Al-Suwaidi et al., 2010; Caruthers et al., 2011; Gröcke et al., 2011). The origin of the generally light $\delta^{13}C_{org}$ values in the Bächental bituminous marls is not yet clear, and several mechanisms are possible. [i] $^{13}C$-depleted OM produced by means of carbon recycling processes mediated by chemoautotrophic and methanotrophic microbes within an anoxic, stratified water column (e.g., Küspert, 1982, 1983; Hollander and Smith, 2001). Biogenic methane oxidation at the oxic/anoxic interface during periods of highest nutrient concentrations in the water column may have reinforced this signal; hence, the level of eutrophication controls the biogeochemical processes that influence $\delta^{13}C_{org}$ compositions (Hollander and Smith, 2001). [ii] Varying contributions of OM from eukaryotic algae, anaerobic chemoautotrophs, and other microbial plankton (e.g., Luo et al., 2014). In that study, chemoautotrophic bacteria were suggested to be the source of strongly $^{13}C$-depleted OM in deepwater environments. [iii] Expandable smectite possibly derived from alteration of volcanic ash is abundant in all samples; hence a contribution of isotopically light $CO_2$ from volcanic emissions is possible.

On the other hand, OM-poor rocks of *Scheibelberg Fm.* and *Upper Allgäu Fm.* show heavier $\delta^{13}C_{org}$ isotope values (-29.4 to -23.6‰ VPDB) that are similar to correlative strata in other Toarcian sections (see above for references) and, hence, were not affected by processes described above. In the case of the lower Toarcian Bächental bituminous marls, the $\delta^{13}C_{carb}$, $\delta^{18}O_{carb}$, and $\delta^{13}C_{org}$ isotopes do not show any correlation. Furthermore, the pronounced negative CIE ($\delta^{13}C_{carb}$ and $\delta^{13}C_{org}$) that characterizes the lower Toarcian globally is missing, questioning its unrestricted applicability as a ubiquitous chemostratigraphic marker for this time interval. The reason for its absence is not yet clear but may be due to overprinting of the global signal by local controls.

### *5.3.3 OM accumulation in Pliensbachian-Toarcian: Oceanic response to magmatic events*

Significant relationships exist between emplacement of LIPs, long-term environmental changes, global climate warming, and extinction events reflected by major geochemical perturbations and increased OM accumulation (“volcanic greenhouse scenario”; Wignall et al., 2005; Caruthers et al., 2013). The end-Triassic release of large quantities of greenhouse gases during the CAMP eruptions (~201 Ma) initiated a significant global warming process during Early Jurassic times (McElwain et al., 1999; McHone, 2003; Cohen and Coe, 2007). Global warming intensified further as a consequence of volcanic activity associated with the rift-related Karoo and Ferrar LIPs (Caruthers et al., 2013) during the Early Jurassic

(Encarnación et al., 1996; Minor and Mukasa, 1997; Svensen et al., 2007, 2012; Sell et al., 2014), resulting in peak "greenhouse Earth" conditions in the Toarcian (Jenkyns and Clayton, 1997; Pálfy and Smith, 2000; Weissert, 2000; Jenkyns, 2003). In addition, several volcanic pulses were associated with complex rifting of the Alpine Tethys ranging from the Late Triassic to the Middle Jurassic (Decarlis et al., 2013). The establishment and intensification of greenhouse climate at that time was possibly supported by the release of methane hydrates (Jenkyns and Clayton, 1997; Hesselbo et al., 2000). In addition, the Karoo-Ferrar volcanism intensified continental weathering and the hydrological cycle (Cohen et al., 2004). The marine ecosystem was affected by alterations of seawater chemistry (Martin and Macdougall, 1995) and development of oceanic anoxia (Harnik et al., 2012). The late Pliensbachian and early Toarcian were characterized by several marine extinction events that were probably triggered by eruptions of the Karoo and Ferrar LIPs (Dera et al., 2010; Caruthers et al., 2013). Although the main phase of extinction occurred within an interval ranging from the Pliensbachian-Toarcian boundary to the lowermost *falciferum* Zone, a significant global extinction pulse is also reported for the late Pliensbachian *margaritatus* Zone, indicating a rapid biotic response to LIP activity (Dera et al., 2010; Caruthers at al., 2013). The combination of these global changes provided conditions favourable to OM accumulation during upper Pliensbachian and lower Toarcian in oceanic settings.

The apparent onset of OM accumulation in the tectonically complex Bächental basin during the late Pliensbachian *margaritatus* Zone (Fig. 13) is consistent with data from other age-equivalent sections in semi-restricted depositional settings, e.g., Cleveland Basin in NW Europe (McArthur et al., 2008) and the Neuquén Basin in Argentina (Al-Suwaidi et al., 2010). This suggests a rapid oceanic response of semi-restricted basins to greenhouse gas emissions, elevated atmospheric $CO_2$ levels, and global climate warming triggered by the Karoo and Ferrar LIPs (cf. Mazzini et al., 2010). Whereas high precision U-Pb data suggest a stratigraphic age of ~183 Ma (equivalent to early Toarcian) for the onset of Karoo volcanism (Svensen et al., 2007, 2012; Sell et al., 2014), the Ferrar LIP was active already at ~184 Ma (equivalent to late Pliensbachian; Encarnación et al., 1996; Minor and Mukasa, 1997). Thus, the early stages of Early Jurassic LIP magmatism may have coincided with the onset of OM accumulation for the above-mentioned sections. In the Alpine Tethyan domain, the establishment of anoxia in Pliensbachian to Toarcian times was linked to local basin geometry, with reducing conditions commencing earlier than the Toarcian in basins that were prone to restriction and water-column stratification (Fig. 14).

The carbonate-free mudstone at the base of the Bächental bituminous marls contains charred organic material typically connected to wildfires (e.g., Brown et al., 2012) and large amounts of expandable smectite possibly derived from alteration of volcanic ash. In contrast, the underlying *Scheibelberg Formation* contains only illite in its clay fraction. This suggests that onset of OM accumulation and establishment of reducing conditions in the Bächental basin were associated with a volcanic event of possibly regional scale in the NW Tethyan domain. Significant amounts of smectite present in all marl samples indicate a pronounced contribution of volcanic-derived detritus during deposition of the Bächental bituminous marls. This is consistent with the occurrence of volcanic ashes and lava flows in the Pliensbachian and Toarcian of the Tethyan domain (Decarlis et al., 2013), the complex rift history of the Valais, Briançonnais and Piemonte-Liguria domains at the proximal European and Adriatic margins between late Sinemurian and Callovian time (Mohn et al., 2010), and the contemporaneous break-up of the Ligurian-Penninic oceanic realm (Ratschbacher et al., 2004).

The main pulses of Karoo and Ferrar LIP magmatism during the upper *tenuicostatum*-lower *falciferum* zones are thought to have triggered the T-OAE on a global scale (e.g., Svensen et al., 2007; Dera et al., 2010; Mazzini et al., 2010; Ikeda and Hori, 2014). The main eruption stage of these LIPs correlates approximately with the base of Subunit 2a (Figs. 2, 13). Subunit 2a accumulated in a restricted basinal setting characterized by strictly anoxic conditions, a salinity-stratified watermass, and a concurrent flourishing of surface-water productivity during a period of relative sea-level lowstand. Hence, local factors (i.e., basin restriction due to eustatic controls) can sufficiently explain environmental conditions controlling bituminous marl sedimentation in the Bächental basin. However, LIP-related perturbations of the carbon cycle triggered global conditions favoring widespread development of marine anoxia that potentially reinforced the local controlling factors in the Bächental basin and triggered rapid OM accumulation in Subunit 2a of the study section.

## 6. Conclusions

The Bächental bituminous marls provide insights into global and local factors controlling the onset and duration of OM accumulation in semi-restricted basins during late Pliensbachian and early Toarcian times.

- A stagnant basin setting during a period of relative sea-level lowstand in Subunit 2a corresponding to the upper *tenuicostatum* and lower *falciferum* zones triggered the

establishment of strong anoxia, a salinity-stratified watermass, and a flourishing of surface-water productivity that jointly enhanced OM accumulation. Hence, redox and salinity changes in the tectonically complex Bächental basin were controlled mainly by minor sea-level fluctuations that resulted in varying watermass exchange and bottom water oxygenation.

- Stratigraphic correlation of the Bächental bituminous marls with the time-equivalent SW German Posidonia Shale suggests that deposition of OM-rich sediments in the Alpine realm commenced earlier (late Pliensbachian *margaritatus* Zone) than in proximal epicontinental areas (early Toarcian *tenuicostatum* Zone) indicating a rapid oceanic response to the major environmental perturbations caused by the activity of Karoo and Ferrar LIPs and complex rifting of the Alpine Tethys in local basins that were prone to the development of water-column stratification and deepwater anoxia because of their geometry or paleogeographic setting. Charred material at the base of the study section suggests that a possibly regional volcanic event was the trigger for onset of OM accumulation. Continued inputs of volcanic detritus during marl deposition confirms volcanic activity during late Pliensbachian and early Toarcian times in the NW Tethyan domain. Intervals with peak TOC contents in the study section probably correspond to the main magmatic stage of the Karoo and Ferrar LIPs, suggesting a massive effect on coeval marine productivity.
- The early Toarcian negative CIE that is observed in age-equivalent sections worldwide is not visible in either the carbonate or organic carbon $\delta^{13}C$ profiles of the study section. Thus, this chemostratigraphic marker cannot be used in correlation of the Bächental bituminous marls. The global CIE appears to have been overprinted owing to local factors in the study section. Consequently, the unrestricted applicability of the early Toarcian negative CIE as a ubiquitous chemostratigraphic marker for the early Toarcian has to be questioned.

## Acknowledgments

We gratefully thank family Albrecht (Tiroler Steinöl ®) who operate the Bächental open pit for their technical support during sampling and Joachim Blau (Giessen) for identification of the ammonite *Cleviceras exaratum*. Research by TJA is supported by the Sedimentary Geology and Paleobiology program of the U.S. National Science Foundation, the

NASA Exobiology program, and the State Key Laboratory of Geological Processes and Mineral Resources, China University of Geosciences, Wuhan (Program GPMR201301).

# Appendix – Full data set for samples of the investigated Bächental section

**Table 1:** Bulk geochemical data for samples of Bächental section.

| Sample | Diag. carb. *[peak area]* | TOC *[%]* | $Cc_{eq}$ *[%]* | S *[%]* | HI *[mg HC/g TOC]* | Fe *[%]* | $\delta^{13}C_{carb}$ *[‰ VPDB]* | $\delta^{18}O_{carb}$ *[‰ VPDB]* | $\delta^{13}C_{org}$ *[‰ VPDB]* |
|---|---|---|---|---|---|---|---|---|---|
| **BT 68** | - | 0.1 | 81.5 | 0.1 | - | 0.2 | -0.1 | -2.1 | -26.7 |
| **BT 67** | - | 0.2 | 43.6 | 0.0 | - | 0.8 | 0.2 | -3.9 | -25.6 |
| **BT 66** | - | 0.3 | 29.9 | 0.0 | - | 2.6 | 0.1 | -5.0 | -26.3 |
| **BT 65** | - | 0.3 | 35.8 | 0.0 | - | 1.5 | -0.7 | -4.9 | -26.0 |
| **BT 64** | - | 0.1 | 82.2 | 0.1 | - | 0. | -0.1 | -1.9 | -27.1 |
| **BT 63** | - | 0.4 | 40.4 | 0.4 | - | 0.6 | -0.8 | -4.2 | -29.4 |
| **BT 62** | - | 0.1 | 71.1 | 0.2 | - | - | -0.8 | -1.8 | -27.6 |
| **BT 61** | - | 0.3 | 43.4 | 0.1 | - | 0.6 | -0.8 | -4.0 | -25.9 |
| **BT 60** | - | 0.3 | 49.6 | 0.2 | - | 0.4 | -0.7 | -3.5 | -26.1 |
| **BT 59** | - | 0.1 | 78.4 | 0.1 | - | - | -0.6 | -2.0 | - |
| **BT 58** | 4990 | 2.8 | 23.2 | 5.4 | 544 | 4.7 | -2.6 | -4.4 | -31.6 |
| **BT 57** | 5080 | 3.0 | 22.8 | 5.8 | 541 | 6.1 | -2.2 | -4.2 | -31.6 |
| **BT 56** | 17590 | 2.1 | 50.8 | 3.4 | 541 | 3.7 | -5.8 | -3.6 | -30.6 |
| **BT 55** | 6250 | 1.6 | 33.3 | 3.2 | 503 | - | -6.0 | -3.8 | - |
| **BT 54** | 17560 | 1.5 | 53.3 | 5.0 | 375 | 1.4 | -7.2 | -3.5 | -26.4 |
| **BT 53** | 14040 | 1.6 | 47.1 | 5.7 | 415 | 4. | -5.6 | -3.2 | -31.1 |
| **BT 52** | 18680 | 1.7 | 52.0 | 5.0 | 419 | 4.0 | -10.8 | -3.1 | -31.2 |
| **BT 51** | 21260 | 1.5 | 55.4 | 2.1 | 362 | 3.4 | -12.7 | -3.0 | -30.9 |
| **BT 50** | 14960 | 1.6 | 56.7 | 1.3 | 325 | 4.9 | -5.2 | -2.1 | -31.1 |
| **BT 49** | 16860 | 1.7 | 52.9 | 2.6 | 292 | - | -6.9 | -2.8 | - |
| **BT 48** | 16510 | 2.1 | 51.0 | 2.5 | 379 | 3.9 | -7.3 | -3.3 | -31.1 |
| **BT 47** | 16900 | 1.6 | 60.7 | 2.0 | 320 | 5.3 | -8.6 | -2.3 | -31.1 |
| **BT 46** | 15200 | 1.5 | 64.8 | 1.9 | 370 | 3.2 | -7.9 | -2.4 | - |
| **BT 45** | 14100 | 1.5 | 56.9 | 2.6 | 400 | 5.2 | -8.3 | -2.5 | -31.1 |
| **BT 44** | 15990 | 1.9 | 48.6 | 5.3 | 350 | 5.4 | -8.7 | -2.7 | -31.0 |
| **BT 43** | - | 0.1 | 82.6 | 0.2 | - | 0.9 | 0.8 | -1.4 | -28.7 |
| **BT 42** | - | 0.1 | 90.8 | 0.0 | - | 0.6 | -0.2 | -1.4 | -29.0 |
| **BT 41** | - | 0.1 | 89.5 | 0.1 | - | 0.8 | -0.2 | -2.3 | -30.1 |
| **BT 40** | 7830 | 3.0 | 36.9 | 3.5 | 604 | 3.5 | -2.5 | -3.8 | -30.6 |
| **BT 39** | 2630 | 5.6 | 38.8 | 5.1 | 683 | 1.1 | -1.5 | -4.0 | -30.9 |
| **BT 38** | 2690 | 5.6 | 32.3 | 5.3 | 661 | 1.9 | -4.2 | -4.7 | -32.1 |
| **BT 37** | 3370 | 6.3 | 18.6 | 4.4 | 622 | 5.2 | -1.8 | -5.1 | -32.7 |
| **BT 36** | 1170 | 2.9 | 35.2 | 5.9 | 572 | 3.9 | -2.7 | -4.3 | -30.9 |
| **BT 35** | 710 | 9.4 | 56.0 | 2.1 | 666 | 1.5 | -2.1 | -3.9 | -32.0 |
| **BT 34** | 2040 | 8.0 | 43.1 | 2.6 | 644 | 0.3 | -2.9 | -4.6 | -31.1 |
| **BT 33** | 2430 | 3.6 | 33.9 | 2.6 | 670 | 3.2 | -2.4 | -4.4 | -30.6 |
| **BT 32** | 2400 | 4.0 | 27.1 | 7.0 | 602 | 6.1 | -2.4 | -4.4 | -31.2 |
| **BT 31** | 470 | 5.4 | 58.8 | 1.3 | 687 | 1.0 | -2.0 | -3.2 | -31.1 |
| **BT 30** | 2840 | 2.9 | 17.4 | 4.3 | 604 | 4.3 | -2.9 | -5.2 | -32.1 |

| Sample | Diag. carb. *[peak area]* | TOC *[%]* | $Cc_{eq}$ *[%]* | S *[%]* | HI *[mg HC/g TOC]* | Fe *[%]* | $\delta^{13}C_{carb}$ *[‰ VPDB]* | $\delta^{18}O_{carb}$ *[‰ VPDB]* | $\delta^{13}C_{org}$ *[‰ VPDB]* |
|---|---|---|---|---|---|---|---|---|---|
| **BT 29** | 740 | 6.8 | 60.7 | 1.6 | 686 | 1.2 | -1.9 | -3.8 | -31.6 |
| **BT 28** | 2520 | 3.5 | 29.2 | 7.1 | 588 | 6.0 | -2.8 | -4.1 | -31.7 |
| **BT 27** | 3070 | 6.0 | 36.8 | 2.8 | 670 | - | -2.9 | -5.1 | - |
| **BT 26** | 2830 | 7.6 | 37.9 | 3.0 | 653 | 0.1 | -3.0 | -4.8 | -31.5 |
| **BT 25** | 580 | 12.9 | 27.2 | 2.9 | 622 | 0.5 | -2.6 | -6.0 | -32.1 |
| **BT 24** | 1830 | 11.7 | 30.7 | 2.8 | 621 | 0.5 | -2.6 | -5.9 | -31.7 |
| **BT 23** | 1360 | 9.0 | 31.1 | 2.7 | 649 | 2.6 | -2.9 | -5.3 | -31.8 |
| **BT 22** | 260 | 8.6 | 38.0 | 3.2 | 645 | 0.2 | -3.0 | -5.4 | -32.2 |
| **BT 21** | 13460 | 1.8 | 43.6 | 4.2 | 519 | 3.5 | -6.3 | -3.7 | -31.0 |
| **BT 20** | 12720 | 2.0 | 40.0 | 4.3 | 495 | 3.6 | -6.2 | -3.6 | -31.1 |
| **BT 19** | 4280 | 3.3 | 31.0 | 5.6 | 612 | 4.0 | -4.0 | -4.0 | -32.0 |
| **BT 18** | 2200 | 2.5 | 32.1 | 2.2 | 577 | 3.3 | -1.8 | -3.9 | -31.0 |
| **BT 17** | 12060 | 1.8 | 42.2 | 4.3 | 537 | 4.2 | -6.9 | -3.6 | -31.5 |
| **BT 16** | 11350 | 2.3 | 34.6 | 3.8 | 497 | 4.4 | -6.3 | -3.4 | -31.6 |
| **BT 15** | 4940 | 1.9 | 30.7 | 5.5 | 427 | 5.2 | -6.1 | -3.4 | -31.7 |
| **BT 14** | 11630 | 1.4 | 39.6 | 5.7 | 306 | 3.5 | -10.0 | -3.5 | -31.5 |
| **BT 13** | 7750 | 1.1 | 43.4 | 3.6 | 307 | 9.2 | -4.7 | -2.3 | -31.6 |
| **BT 12** | 3820 | 2.2 | 24.4 | 5.3 | 518 | 4.2 | -3.2 | -3.9 | -32.0 |
| **BT 11** | 13820 | 1.8 | 34.1 | 3.7 | 441 | 4.8 | -6.9 | -3.8 | -32.0 |
| **BT 10** | 13750 | 1.8 | 31.2 | 5.5 | 452 | 5.2 | -8.7 | -3.5 | -31.7 |
| **BT 9** | 12200 | 1.6 | 32.9 | 5.4 | 459 | 4.8 | -9.8 | -3.6 | -31.6 |
| **BT 8** | - | 1.8 | 0.6 | 0.1 | 37 | 11.7 | -26.0 | -24.3 | - |
| **BT 7** | - | 1.8 | 1.0 | 0.1 | 74 | 21.9 | -23.5 | -22.9 | -28.7 |
| **BT 6** | - | 0.1 | 87.5 | 1.1 | - | 0.3 | 1.5 | -1.4 | -23.6 |
| **BT 5** | - | 0.1 | 89.8 | 0.1 | - | 0.0 | 0.9 | -1.4 | -26.9 |
| **BT 4** | - | 0.1 | 76.2 | 0.1 | - | 0.0 | 0.8 | -2.3 | -25.8 |
| **BT 3** | - | 0.1 | 84.2 | 0.5 | - | 0.0 | 1.0 | -1.6 | -27.4 |
| **BT 2** | - | 0.1 | 80.4 | 0.1 | - | 0.0 | 1.0 | -1.6 | -26.3 |
| **BT 1** | - | 0.1 | 90.2 | 0.0 | - | - | 1.4 | -1.2 | - |

**Table 2:** Organic geochemical data for investigated bituminous marls of Bächental section.

| Sample | *n*-$C_{15-19}$/ Σ*n*-alkanes *[rel. prop.]* | *n*-$C_{27-31}$/ Σ*n*-alkanes *[rel. prop.]* | Pr/Ph *[conc. ratios]* | $C_{27}/C_{29}$ ααα**R** Steranes *[conc. ratios]* | $C_{27}/C_{29}$ Steranes *[conc. ratios]* | 4-Methylsteranes/ $C_{29}$ Steranes *[conc. ratios]* |
|---|---|---|---|---|---|---|
| **BT58** | 0.30 | 0.16 | 1.39 | 0.59 | 0.59 | 0.74 |
| **BT 55** | 0.30 | 0.16 | 1.76 | 0.76 | 1.03 | 1.00 |
| **BT 50** | 0.33 | 0.15 | 1.73 | 0.62 | 0.88 | 0.92 |
| **BT 45** | 0.34 | 0.15 | 1.59 | 0.66 | 0.91 | 1.08 |
| **BT 44** | 0.31 | 0.16 | 0.88 | 0.70 | 0.76 | 2.55 |
| **BT 40** | 0.34 | 0.16 | 1.30 | 0.75 | 1.01 | 1.34 |
| **BT 39** | 0.22 | 0.20 | 0.92 | 0.81 | 1.10 | 1.68 |
| **BT 37** | 0.32 | 0.15 | 1.06 | 0.56 | 0.77 | 1.16 |
| **BT 36** | 0.24 | 0.19 | 0.89 | 0.75 | 0.97 | 1.04 |
| **BT 35** | 0.56 | 0.02 | 0.93 | 0.56 | 0.57 | 3.10 |
| **BT 33** | 0.30 | 0.16 | 0.73 | 0.73 | 0.95 | 1.81 |
| **BT 31** | 0.35 | 0.13 | 0.76 | 0.60 | 0.77 | 2.80 |
| **BT 30** | 0.25 | 0.22 | 0.76 | 0.54 | 0.68 | 1.50 |
| **BT 29** | 0.39 | 0.11 | 0.78 | 0.51 | 0.62 | 2.89 |
| **BT 28** | 0.34 | 0.15 | 0.70 | 0.56 | 0.77 | 2.14 |
| **BT 26** | 0.34 | 0.13 | 0.76 | 0.57 | 0.68 | 2.90 |
| **BT 25** | 0.52 | 0.09 | 1.01 | 0.52 | 0.58 | 3.22 |
| **BT 24** | 0.32 | 0.21 | 0.86 | 0.57 | 0.64 | 3.06 |
| **BT 23** | 0.23 | 0.32 | 0.82 | 0.50 | 0.57 | 2.39 |
| **BT 22** | 0.31 | 0.17 | 0.80 | 0.50 | 0.59 | 2.79 |
| **BT 20** | 0.34 | 0.17 | 1.33 | 0.60 | 0.83 | 1.72 |
| **BT 18** | 0.27 | 0.16 | 1.35 | 0.91 | 1.24 | 1.95 |
| **BT 15** | 0.33 | 0.16 | 1.80 | 0.74 | 0.97 | 0.89 |
| **BT 12** | 0.30 | 0.16 | 0.96 | 0.69 | 0.79 | 2.24 |
| **BT 10** | 0.31 | 0.18 | 1.08 | 0.60 | 0.79 | 1.56 |
| **BT 8** | 0.23 | 0.24 | 0.94 | 0.59 | 0.70 | 2.10 |

**Table 3:** Organic geochemical data for investigated bituminous marls of Bächental section.

| Sample | Mono-/triaromatic Steroids *[conc. ratios]* | Steranes [S/(S+R)] *[conc. ratios]* | DBT/Phen *[conc. ratios]* | Gammacerane Index *[conc. ratios]* | Hopanes [S/(S+R)] *[conc. ratios]* | Aryl-Isoprenoids *[µg/g TOC]* |
|---|---|---|---|---|---|---|
| **BT 58** | 3.39 | 0.11 | 0.32 | 0.07 | 0.80 | 107.65 |
| **BT 55** | 3.41 | 0.10 | 0.23 | 0.05 | 0.73 | 52.76 |
| **BT 50** | 3.16 | 0.12 | 0.30 | 0.12 | 0.92 | 37.93 |
| **BT 45** | 2.68 | 0.11 | 0.48 | 0.16 | 0.93 | 25.00 |
| **BT 44** | 1.64 | 0.32 | 0.46 | 0.59 | 1.16 | 112.14 |
| **BT 40** | 3.15 | 0.12 | 0.48 | 0.17 | 0.80 | 52.61 |
| **BT 39** | 2.98 | 0.12 | 0.46 | 0.16 | 0.77 | 62.17 |
| **BT 37** | 2.94 | 0.11 | 0.49 | 0.09 | 0.78 | 5.76 |
| **BT 36** | 2.55 | 0.14 | 0.60 | 0.14 | 0.91 | 69.93 |
| **BT 35** | 1.48 | 0.23 | 0.75 | 0.80 | 1.33 | 33.65 |
| **BT 33** | 2.17 | 0.29 | 0.69 | 0.41 | 1.0 | 54.14 |
| **BT 31** | 1.34 | 0.31 | 0.76 | 0.63 | 1.43 | 15.54 |
| **BT 30** | 1.74 | 0.30 | 0.78 | 0.27 | 1.27 | 28.82 |
| **BT 29** | 1.29 | 0.32 | 0.83 | 0.77 | 1.72 | 10.92 |
| **BT 28** | 1.61 | 0.31 | 0.78 | 0.39 | 1.35 | 10.03 |
| **BT 26** | 1.31 | 0.33 | 0.75 | 0.71 | 1.42 | 9.31 |
| **BT 25** | 1.33 | 0.25 | 0.78 | 0.77 | 1.28 | 84.01 |
| **BT 24** | 1.41 | 0.32 | 0.72 | 0.72 | 1.25 | 21.20 |
| **BT 23** | 1.54 | 0.28 | 0.64 | 0.55 | 1.21 | 15.59 |
| **BT 22** | 1.25 | 0.28 | 0.78 | 0.75 | 1.46 | 9.63 |
| **BT 20** | 2.91 | 0.11 | 0.46 | 0.13 | 0.79 | 27.82 |
| **BT 18** | 3.81 | 0.18 | 0.23 | 0.15 | 0.81 | 8.01 |
| **BT 15** | 3.78 | 0.11 | 0.25 | 0.05 | 0.77 | 3.15 |
| **BT 12** | 2.07 | 0.27 | 0.29 | 0.53 | 1.01 | 22.88 |
| **BT 10** | 2.06 | 0.16 | 0.33 | 0.37 | 0.99 | 13.31 |
| **BT 8** | 1.68 | 0.23 | 0.38 | 0.58 | 1.11 | 1.26 |

# References


Algeo, T.J., Wilkinson, B.H., Lohmann, K.C., 1992. Meteoric-burial diagenesis of Pennsylvanian carbonate: water/rock interactions and basin geothermics. Journal of Sedimentary Petrology 62, 652-670.

Al-Suwaidi, A.H., Angelozzi, G.N., Baudin, F., Damborenea, S.E., Hesselbo, S.P., Jenkyns, H.C., Manceñido, M.O., Riccardi, A.C., 2010. First record of the Early Toarcian Oceanic Anoxic Event from the Southern Hemisphere, Neuquén Basin, Argentina. Journal of the Geological Society, London 167, 633-636.

Arthur, M.A., Sageman, B.B., 1994. Marine black shales: Depositional mechanisms and environments of ancient deposits. Annual Review of Earth and Planetary Sciences 2, 126-166.

Auras, S., Püttmann, W., 2004. Zusammensetzung und Herkunft der 4-Methylsteroide im Messeler Ölschiefer. Cour. Forsch.-Inst. Senckenberg 252, 139-149.

Barakat, A.O., Rullkötter, J., 1997. A comparative study of molecular paleosalinity indicators: chromans, tocopherols and $C_{20}$ isoprenoid thiophenes in Miocene lake sediments (Nördlinger Ries, Southern Germany). Aquatic Geochemistry 3, 169-190.

Bechtel, A., Jia, J., Strobl, S.A.I., Sachsenhofer, R.F., Liu, Z., Gratzer, R., Püttmann, W., 2012. Palaeoenvironmental conditions during deposition of the Upper Cretaceous oil shale sequences on the Songliao Basin (NE China): Implications from geochemical analysis. Organic Geochemistry 46, 76-95.

Berner, R.A., 1970. Sedimentary pyrite formation. Am. J. Sci. 268, 1-23.

Berner, R.A., 1984. Sedimentary pyrite formation: An update. Geochimica et Cosmochimica Acta 48, 605-615.

Berner, R.A., Raiswell, R., 1983. Burial of organic carbon and pyrite sulfur in sediments over Phanerozoic time: A new theory. Geochimica et Cosmochimica Acta 47, 862-885.

Bernoulli, D., Jenkyns, H.C., 1974. Alpine, Mediterranean and Central Atlantic Mesozoic facies in relation to the early evolution of the Tethys. In: Dott, R.H., Shaver, R.H. (Eds.), Modern and Ancient Geosynclinal Sedimentation, a Symposium. Special Publication of the Society of economic Paleontologists and Mineralogists 19,129-160.

Bernoulli, D., Jenkyns, H.C., 2009. Ancient oceans and continental margins of the Alpine-Mediterranean Tethys: deciphering clues from Mesozoic pelagic sediments and ophiolites. Sedimentology 56,149-190.

Blumenberg, M., Krüger, M., Nauhaus, K., Talbot, H.M., Oppermann, B., Seifert, R., Pape, T., Michaelis, W., 2006. Biosynthesis of hopanoids by sulfate-reducing bacteria (genus Desulfovibrio). Environ. Microbiol. 8, 1220-1227.

Bray, E.E., Evans, E.D., 1961. Distribution of n-paraffins as a clue to recognition of source beds. Geochimica et Cosmochimica Acta 22, 2-15.

Brandner, R., 2011. In: Geologie des Achenseegebiets. Tagungsband der Arbeitstagung der Geologischen Bundesanstalt, Wien: 220-224.

Brown, S.A.E., Scott, A.C., Glasspool, I.J., Collinson, M.E., 2012. Cretaceous wildfires and their impact on the Earth system. Cretaceous Research 36, 162-190.

1054 Calvert, S.E., Pedersen, T.F., 1996. Sedimentary Geochemistry of Manganese: Implications for the Environment
1055 of Formation of Manganiferous Black Shales. Economic Geology 91, 36-47.

1056 Caruthers, A.H., Gröcke, D.R., Smith, P.L., 2011. The significance of an Early Jurassic (Toarcian) carbon-
1057 isotope excursion in Haida Gwaii (Queen Charlotte Islands), British Columbia, Canada. Earth and
1058 Planetary Science Letters 307, 19-26.

1059 Caruthers, A.H., Smith, P.L., Gröcke, D.R., 2013. The Pliensbachian-Toarcian (Early Jurassic) extinction, a
1060 global multi-phased event. Palaeogeography, Palaeoclimatology, Palaeoecology 386, 104-118.

1061 Cohen, A.S., Coe, A.L., 2007. The impact of the Central Magmatic province on climate and on the Sr- and Os-
1062 isotope evolution of seawater. Palaeogeography, Palaeoclimatology, Palaeoecology 244, 374-390.

1063 Cohen, A.S., Coe, A.L., Harding, S.M., Schwark, L., 2004. Osmium isotope evidence for the regulation of
1064 atmospheric $CO_2$ by continental weathering. Geology 32, 157-160.

1065 Cranwell, P.A., 1977. Organic geochemistry of CamLoch (Sutherland) sediments. Chemical Geology 20, 205-
1066 221.

1067 Dean, W.E., Arthur, M.A., 1989. Iron-sulfur-carbon relationships in organic-rich sequences. In: Cretaceous
1068 Western Interior Seaway. American Journal of Science 289, 708-743.

1069 Decarlis, A., Dallagiovanna, G., Lualdi, A., Maino, M., Seno, S., 2013. Stratigraphic evolution in the Ligurian
1070 Alps between Variscian heritages and the Alpine Tethys opening: A review. Earth-Science Reviews 125,
1071 43-68

1072 Demaison, G.J., Moore, G.T., 1980. Anoxic environments and oil source bed genesis. AAPG Bulletin 64, 1179-
1073 1209.

1074 Dera, G., Neige, P., Dommergues, J.-L., Fara, E., Laffont, R., Pellenard, P., 2010. High-resolution dynamics of
1075 Early Jurassic marine extinctions: the case of Pliensbachian–Toarcian ammonites (Cephalopoda). J. Geol.
1076 Soc. (Lond.) 167, 21–33.

1077 Didyk, B.M., Simoneit, B.R.T., Brassell, S.C., Eglinton, G., 1978. Organic geochemical indicators of
1078 palaeoenvironmental conditions of sedimentation. Nature 272, 216-222.

1079 Ebli, O., 1991. Beiträge von Draxler, I., Klein, P., Kodina, L.A., Lobitzer, H., Schwaighofer, B. Fazies,
1080 Paläontologie und organische Geochemie der Sachranger Schiefer (Untertoarcium) im Mittelabschnitt der
1081 Nördlichen Kalkalpen zwischen Isar und Saalach. Jahrbuch der Geologischen Bundesanstalt 134/1, 5-14.

1082 Ebli, O., Vetö, I., Lobitzer, H., Sajgò, C., Demény, A., Hetényi, M., 1998. Primary productivity and early
1083 diagenesis in the Toarcian Tethys on the example of the Mn rich black shales of the Sachrang Formation,
1084 Northern Calcareous Alps. Organic Geochemistry 29, 1635-47.

1085 Encarnación, J., Fleming, T.H., Elliot, D.H., Eales, H.V., 1996. Synchronous emplacement of Ferrar and Karoo
1086 dolerites and the early breakup of Gondwana. Geology 24, 535-538.

1087 Espitalié, J., Marquis, F., Barsoni, I., 1984. Geochemical logging. In: Voorhess, K.J. (Eds.), Analytical Pyrolysis.
1088 Butterworth, Boston. pp. 53-79.

1089 Fabricus, F., 1966. Beckensedimentation und Riffbildung an der Wende Trias/Jura in den Bayrisch-Tiroler
1090 Kalkalpen. Internat. Sedim. Petrogr. Series 9, 143 S.

1091 Faupl, P., Wagreich, M., 2000. Late Jurassic to eocene palaeogeography and geodynamic evolution of the
1092 Eastern Alps. Mitteilungen der Österreichischen Geologischen Gesellschaft 92, 79-94.

1093 Frimmel, A., Oschmann, W., Schwark, L., 2004. Chemostratigraphy of the Posidonia Shale, SW Germany I.
1094 Influence of sea-level variation on organic facies evolution. Chemical Geology 206, 199-230.

1095 Frisch, W., 1979. Tectonic Progradation on plate tectonic evolution of the Alps. Tectonophysics 60, 121-139.

1096 Frisch, W., Gawlick, H.-J., 2003. The nappe structure of the central Northern Calcareous Alps and its
1097 disintegration during Miocene tectonic extrusion – a contribution to understanding the orogenic evolution
1098 of the Eastern Alps. International Journal of Earth Sciences 92, 712-727.

1099 Frisch, W., Meschede, M., Blakey, R., 2011. Plate Tectonics. Springer, pp. 112.

1100 Fu, J.G., Sheng, P., Peng, S.C., Brassell, S.C., Eglington, G., 1986. Pecularities of salt lake sediments as
1101 potential source rocks in China. Organic Geochemistry 10, 119-127.

1102 Gawlick, H.-J., Frisch, W., Hoxha, L., Dumitrica, P., Krystyn, L., Lein, R., Missoni, S., Schlagintweit, F., 2008.
1103 Mirdita Zone ophiolites and associated sediments in Albania reveal Neotethys Ocean origin. International
1104 Journal of Earth Sciences 97, 865-881.Gawlick, H-J., Missoni, S., Schlagintweit, F., Suzuki, H., Frisch,
1105 W., Krystyn, L., Blau, J., Lein, R., 2009. Jurassic Tectonostratigraphy of the Austroalpine Domain.
1106 Journal of Alpine Geology 50: 1-152.

1107 Golonka, J., 2002. Plate-tectonic Maps of the Phanerozoic. In: Kiessling, W., Flu□gel, E., Golonka, J. (Eds.),
1108 Phanerozoic Reef Patterns. SEPM Special Publication 72, 21-75.

1109 Goossens, H., de Leeuw, J.W., Schenck, P.A., Brassell, S.C., 1984. Tocopherols as likely precursors of pristane
1110 in ancient sediments and crude oils. Nature 312, 440-442.

1111 Gradstein, F.M., Ogg, J.G., Schmitz, M.D., et al., 2012. The Geologic Time Scale 2012. Elsevier, Boston.

1112 Grantham, P.J., Posthuma, J., Baak, A., 1983. Triterpanes in a number Far Eastern crude oils. In: Bjoroy, M., et
1113 al. (Eds.), Advances in Organic Geochemistry. Wiley, Chichester. pp. 675-683.

1114 Grice, K., Gibbison, R., Atkinson, J.E., Schwark, L., Eckardt, C.B.E., Maxwell, J.R., 1996. Maleimides (1H-
1115 pyrrole-2,5-diones) as indicators of anoxygenic photo-synthesis in ancient water columns. Geochim.
1116 Cosmochim. Acta 60, 3913-3924.

1117 Gröcke, D.R., Hori, R.S., Trabucho-Alexandre, J., Kemp, D.B., Schwark, L., 2011. An open ocean record of the
1118 Toarcian oceanic anoxic event. Solid Earth 2, 245-57.

1119 Hallam, A., 1992. Phanerozoic Sea-level Changes. Columbia University Press, New York. pp. 266.

1120 Harnik, P.G., Lotze, H.K., Anderson, S.C., Finkel, Z.V., Finnegan, S., Lindberg, D.R., Liow, L.H., Lockwood,
1121 R., McClain, C.R., McGuire, J.L., O`Dea, A., Pandolfi, J.M., Simpson, C., Tittensor, D.P., 2012.
1122 Extinctions in ancient and modern seas. Trends in Ecology and Evolution 27, 608-617.

1123 Haq, B.U., Hardenbol, J., Vail, P.R., 1988. Mesozoic and Cenozoic chronostratigraphy and cycles of sea-level
1124 change. In: Wilgus, C.K., Hastings, B.S., Posamentier, H., Wagoner, J.V., Ross, C.A., Kendall, C.G.S.C.
1125 (Eds.), Sea-Level Changes - An Integrated Approach. SEPM Special Publications 42, 71-108.

1126 Hesselbo, S.P., Gröcke, D.R., Jenkyns, H.C., Bjerrum, C.J., Farrimond, P., Morgans Bell, H.S., Green, O.R.,
1127 2000. Massive dissociation of gas hydrate during a Jurassic oceanic anoxic event. Nature 406, 392-395.

1128 Hesselbo, S.P., Jenkyns, H.C., Duarte, L.V., Oliviera, L.C.V., 2007. Carbon-isotope record of the Early Jurassic
1129 (Toarcian) Oceanic Anoxic Event from fossil wood and marine carbonate (Lusitanian Basin, Portugal).
1130 Earth and Planetary Science Letters 253, 455-470.

1131 Hofmann, P., Ricken, W., Schwark, L., Leythaeuser, D., 2000. Carbon–sulfur–iron relationships and $\delta^{13}C$ of
1132 organic matter for Late Albian sedimentary rocks from the North Atlantic Ocean: Palaeoceanographic
1133 implications. Palaeogeography, Palaeoclimatology, Palaeoecology 163 (3-4), 97-113.

1134 Hollander, D.J., Smith, M.A., 2001. Microbially mediated carbon cycling as a control on the d13C of
1135 sedimentary carbon in eutrophic Lake Mendota (USA): new models for interpreting isotopic excursions in
1136 the sedimentary record. Geochimica et Cosmochimica Acta 65, 4321-4337.

1137 Hughes, W.B., Holba, A.G., Dzou, L.I.P., 1995. The ratios of dibenzothiophene to phenanthrene and pristane to
1138 phytane as indicators of depositional environment and lithology of petroleum source rocks. Geochimica et
1139 Cosmochimica Acta 59, 3581-3598.

1140 Hutton, A.C., 1987. Petrographic classification of oil shales. Internat. J. Coal Geol. 8, 203-231.

1141 Ikeda, M., Hori, R.S., 2014. Effects of Karoo-Ferrar volcanism and astronomical cycles on the Toarcian Anoxic
1142 Events (Early Jurassic). Palaeogeography, Palaeoclimatology, Palaeoecology 410, 134-142.

1143 Irwin, H., Curtis, C.D., Coleman, M., 1977. Isotopic evidence for source of diagenetic carbonates formed during
1144 burial of organic-rich sediments. Nature 269, 209-213.

1145 Izumi, K., Miyaji, T., Tanabe, K., 2012. Early Toarcian (Early Jurassic) oceanic anoxic event recorded in the
1146 shelf deposits in the northwestern Panthalassa: Evidence from the Nishinakayama Formation in the
1147 Toyora area, west Japan. Palaeogeography, Palaeoclimatology, Palaeoecology 315-316, 100-108.

1148 Jaminski, J., Algeo, T.J., Maynard, J.B., Hower, J.C., 1998. Climatic origin of dm-scale compositional cyclicity
1149 in the Cleveland Member of the Ohio Shale (Upper Devonian), Central Appalachian Basin, U.S.A. In:
1150 Schieber, J., Zimmerle, W., Sethi, P.S. (Eds.), Shales and Mudstones. I.E. Schweizerbart'sche
1151 Verlagsbuchhandlung, Stuttgart. pp. 217-242.

1152 Jenkyns H. C., 1985. The Early Toarcian and Cenomanian–Turonian anoxic events in Europe: comparisons and
1153 contrasts. Geologische Rundschau 74, 505-518.

1154 Jenkyns, H.C., 1988. The Early Toarcian (Jurassic) anoxic event: stratigraphic, sedimentary, and geochemical
1155 evidence. American Journal of Science 288, 101-151.

1156 Jenkyns, H.C., 2003. Evidence for rapid climate change in the Mesozoic–Palaeogene greenhouse world.
1157 Philosophical Transactions of the Royal Society of London 361 A, 1885-1916.

1158 Jenkyns, H.C., 2010. The geochemistry of oceanic anoxic events. Geochemistry Geophysics Geosystems 11,
1159 Q03004, doi: 10.1029/2009GC002788.

1160 Jenkyns, H.C., Clayton, C.J., 1986. Black shales and carbon isotopes in pelagic sediments from the Tethyan
1161 Lower Jurassic. Sedimentology 33, 87-106.

1162 Jenkyns, H.C., Clayton, C.J., 1997. Lower Jurassic epicontinental carbonates and mudstones from England and
1163 Wales: chemostratigraphic signals and the early Toarcian anoxic event. Sedimentology 44, 687-706.

1164 Jenkyns, H.C., Gröcke, D.R., Hesselbo, S.P., 2001. Nitrogen isotope evidence for water mass denitrification
1165 during the early Toarcian (Jurassic) ocean anoxic event. Paleoceanography 16, 593–603.

1166 Jenkyns, H.C., Jones, C.E., Gröcke, D.R., Hesselbo, S.P., Parkinson, D.N., 2002. Chemostratigraphy of the
1167 Jurassic System: applications, limitations and implications for palaeoceanography. Journal of the
1168 Geological Society of London 159, 351-378.

1169 Jourdan, F., Féraud, G., Bertrand, H., Watkeys, M.K., Renne, P.R., 2008. The $^{40}Ar/^{39}Ar$ ages of the sill complex
1170 of the Karoo large igneous province: implications for the Pliensbachian-Toarcian climate change.
1171 Geochemistry, Geophysics, Geosystems 9, 1-20.

1172 Kafousia, N., Karakitsios, V., Mattioli, E., Kenjo, S., Jenkyns, H.C., 2014. The Toarcian Oceanic Anoxic Event
1173 in the Ionian Zone, Greece. Palaeogeography, Palaeoclimatology, Palaeoecology 393, 135-145.

1174 Kemp, D.B., Coe, A.L., Cohen, A.S., Schwark, L., 2005. Astronomical pacing of methane release in the early
1175 Jurassic period. Nature 437, 396-399.

1176 Klebelsberg, R.v., 1935. Geologie von Tirol. Gebr. Borntraeger, Berlin.

1177 Kodina, L.A., Bogatecheva, M.P., Lobitzer, H., 1988. An anorganic geochemical study of Austrian bituminous
1178 rocks. Jb. Geol. B.-A. 131, 291-300, Wien.

1179 Kohnen, M.E.L., Sinninghe Damsté, J.S., de Leeuw, J.W., 1991. Biases from natural sulphurization in
1180 palaeoenvironmental reconstruction based on hydrocarbon biomarker distributions. Nature 349, 775-778.

1181 Koopmans, M.P., Köster, J., van Kaam-Peters, H.M.E., Kenig, F., Schouten, S., Hartgers, W.A., de Leeuw, J.W.,
1182 Sinninghe Damsté, J.S., 1996. Diagenetic and catagenetic products of isorenieratene: molecular indicators
1183 for photic zone anoxia. Geochim. Cosmochim. Acta 60, 4467-4496.

1184 Köster, J., Schouten, S., Sinninghe Damsté, J.S.de Leeuw, J.W., 1995. Reconstruction of the depositional
1185 environment of Toarcian marlstones (Allgäu Formation, Tyrol/Austria) using biomarkers and compound
1186 specific carbon isotope analysis. In: Grimalt, J.O., Dorronsoro, C. (Eds.), Organic Geochemistry:
1187 Developments and applications to energy, climate, environment and human history. A.I.G.O.A., San
1188 Sebastian. pp. 76-78.

1189 Kuehl, S.A., Fuglseth, T.J., Thunell, R.C., 1993. Sediment mixing and accumulation rates in the Sulu and South
1190 China Seas: Implications for organic carbon preservation in deep-water environments. Mar. Geol. 111,
1191 15-35.

1192 Küspert, W., 1982. Environmental changes during oil shale deposition as deduced from stable isotope ratios. In:
1193 Einsele, G., Seilacher, A. (Eds.), Cyclic and Event Stratification. Springer, Berlin. pp. 482-501.

1194 Küspert, W., 1983. Faziestypen des Posidonienschiefers (Toarcium, Süddeutschland): Eine isotopen-
1195 geologische, organisch-chemische und petrographische Studie. Ph.D. Thesis, Tübingen University.

1196 Langford, F.F., Blanc-Valleron, M.-M., 1990. Interpreting Rock-Eval pyrolysis data using graphs of pyrolyzable
1197 hydrocarbons vs. total organic carbon. American Association of Petroleum Geologists Bulletin 74, 799-
1198 804.

1199 Leventhal, J.S., 1983. An interpretation of carbon and sulfur relationships in Black Sea sediments as indicators
1200 of environments of deposition. Geochimi. Cosmochimi. Acta 47, 133-137.

1201 Lewan, M.D., 1986. Stable carbon isotopes of amorphous kerogens from Phanerozoic sedimentary rocks.
1202 Geochim. Cosmochim. Acta 50, 1583-1591.

1203 Littke, R., Rotzal, H., Leythaeuser, D., Baker, D.R., 1991. Organic facies and maturity of Lower Toarcian
1204 Posidonia Shale in Southern Germany (Schwäbische Alb). Erdöl & Kohle Erdgas
1205 Petrochemie/Hydrocarbon Technology 44, 407-414.

1206 Luo, G.M., Algeo, T.J., Zhou, W.F., Wang, Y.B., Yang, H., Huang, J.H., Richoz, S., Xie, S.C., 2014. Vertical
1207 $\delta^{13}C_{org}$ gradients record changes in planktonic microbial community composition during the end-Permian
1208 mass extinction. Palaeogeography Palaeoclimatology Palaeoecology 396, 119-131.

1209 Mackenzie, A.S., Maxwell, J.R., 1981. Assessment of thermal maturation in sedimentary rocks by molecular
1210 measurements. In: Brooks, J. (Eds.), Organic Maturation Studies and Fossil Fuel Exploration. Academic
1211 Press, London. pp. 239-254.

1212 Mackenzie, A.S., Brassell, SC., Eglinton, G., Maxwell, J.R., 1982. Chemical fossils: the geological fate of
1213 steroids. Science 217, 491-504.

1214 Mangini, A., Dominik, J., 1979. Late Quaternary sapropel on the Mediterranean ridge: U-budget and evidence
1215 for low sedimentation rates. Sedim. Geol. 23, 113-125.

1216 Martin, E.E., Macdougall, J.D., 1995. Sr and Nd isotopes at the Permian Triassic Boundary – a record of climate
1217 change. Chemical Geology 125, 73-99.

1218 Marzoli, A., Renne, P.R., Piccirillo, E.M., Ernesto, M., Bellieni, G., De Min, A., 1999. Extensive 200 million-
1219 year-old continental flood basalts of the central Atlantic magmatic province. Science 284, 616-618.

1220 Mazzini, A., Svensen, H., Leanza, H.A., Corfu, F., Planke, S., 2010. Early Jurassic shale chemostratigraphy and
1221 U–Pb ages from the Neuquén Basin (Argentina): implications for the Toarcian Oceanic Anoxic Event.
1222 Earth Planet. Sci. Lett. 297, 633–645.

1223 McArthur, J.M., Algeo, T.J., van de Schootbrugge, B., Li, Q., Howarth, R.J., 2008. Basinal restriction, black
1224 shales, Re–Os dating, and the Early Toarcian (Jurassic) oceanic anoxic event. Paleoceanography 23, 1–
1225 22.

1226 McElwain, J.C., Beerling, D.J., Woodward, F.I., 1999. Fossil plants and global warming at the Triassic-Jurassic
1227 boundary. Science 285, 1386-1390.

1228 McElwain, J.C., Murphy, J.W., Hesselbo, S.P., 2005. Changes in carbon dioxide during an oceanic anoxic event
1229 linked to intrusion of Gondwana coals. Nature 435, 479-483.

McHone, J.G., 2003. Volatile Emissions from Central Atlantic Magmatic Province Basalts: Mass Assumptions and Environmental Consequences. In: Hames, W.E., McHone, J.G., Ruppel, C., Renne, P. (Eds.), The Central Atlantic Magmatic Province. American Geophysical Union Monograph. pp 136: 267.

Minor, D.R., Mukasa, S.B., 1997. Zircon U-Pb and hornblende $^{40}Ar$-$^{39}Ar$ ages for the Dufek layered mafic intrusion, Antarctica: Implications for the age of the Ferrar large igneous province. Geochimica and Cosmochimica Acta 61, 2497-2504.

Missoni, S., Gawlick, H.-J., 2011. Evidence for Jurassic subduction from the Northern Calcareous Alps (Berchtesgaden; Austroalpine, Germany). International Journal of Earth Sciences 100, 1605-1631.

Mohn, G., Manatschal, G., Müntener, O., Beltrando, M., Masini, E., 2010. Unravelling the interaction between tectonic and sedimentary processes during lithospheric thinning in the Alpine Tethys margins. Int. J. Earth Sci. (Geol. Rundsch.) 99, 75-101.

Morard, A., Guex, J., Bartolini, A., Morettini, E., De Wever, P., 2003. A new scenario for the Domerian-Toarcian transition. Bulletin de la Société géoloique France 174, 351-356.

O'Neil, J.R., Clayton, R.N., Mayeda, T.K., 1969. Oxygen isotope fractionation in divalent metal carbonates. J. Chem. Phys. 51, 5547-5558.

Oschmann, W., 2000. Microbes and black shales. In: Riding, R.E., Awramik, S.M. (Eds.), Microbial Sediments. Springer, Berlin, pp. 137-148.

Ourrison, G, Albrecht, P, Rohmer, M., 1979. The hopanoids: palaeo-chemistry and biochemistry of a group of natural products. Pure and Applied Chemistry 51: 709-729.

Pálfy, J., Smith, P.L., 2000. Synchrony between Early Jurassic extinction, oceanic anoxic event, and the Karoo–Ferrar flood basalt volcanism. Geology 28, 747-750.

Parrish, J.T., 1993. Climate of the supercontinent Pangaea. Journal of Geology 101, 215-233.

Parrish, J.T., Curtis, R.L., 1982. Atmospheric circulation, upwelling, and organic-rich rocks in the Mesozoic and Cenozoic areas. Palaeogeography, Palaeoclimatology, Palaeoecology 40, 31-66.

Pearce, C.R., Cohen, A.S., Coe, A.L., Burton, K.W., 2008. Molybdenum isotope evidence for global ocean anoxia coupled with perturbations to the carbon cycle during the Early Jurassic. Geology 36, 231-234.

Pedersen, T.F., Calvert, S.E., 1990. Anoxia vs. productivity: What controls the formation of organic-carbon-rich sediments and sedimentary rocks? AAPG Bulletin 74, 454-472.

Peters, K.E., Moldowan, J.M., Sundararaman, P., 1990. Effects of hydrous pyrolysis on biomarker thermal maturity parameters: Monterey Phosphatic and Siliceous Members. Organic Geochemistry 15, 249-265.

Peters, K.E., Walters, C.C., Moldowan, J.M., 2005. The Biomarker Guide, Biomarkers and Isotopes in Petroleum Exploration and Earth History, Vol. 1 & 2. Cambridge University Press, New York, NY.

Praus, M., Riegel, W., 1989. Evidence from phytoplanktonic associations for causes of black shale formation in epicontinental seas. N. Jb. Geol. Paläontol. Mh. 11, 671-682.

Price, G.D., 1999. The evidence and implications of polar ice during the Mesozoic. Earth Science Reviews 48, 183-210.

1266 Radke, M., Willsch, H., Welte, D.H., 1980. Preparative hydrocarbon group type determination by automated
1267 medium pressure liquid chromatography. Analytical Chemistry 52, 406-411.

1268 Raiswell, R., Berner, R.A., 1985. Pyrite formation in euxinic and semi-euxinic sediments. Am. J. Sci. 285, 710-
1269 724.

1270 Raiswell, R., Canfield, D.E., Berner, R.A., 1994. A comparison of iron extraction methods for the determination
1271 of degree of pyritisation and the recognition of iron-limited pyrite formation. Chem. Geol. 111, 101-110.

1272 Ratschbacher, L., Dingeldey, C., Miller, C., Hacker, B.R., McWilliams, M.O., 2004. Formation, subduction, and
1273 exhumation of Penninic oceanic crust in the Eastern Alps: time constraints from $^{40}Ar/^{39}Ar$ geochronology.
1274 Tectonophysics 394, 155-170.

1275 Riegraf, W., Werner, G., Lörcher, F., 1984. Der Posidonienschiefer: Biostratigraphie, Fauna und Fazies des
1276 südwestdeutschen Untertoarciums (Lias ε). Enke. pp. 195.

1277 Riegraf, W., 1985. Mikrofauna, Biostratigraphie und Fazies im Unteren Toarcium Südwestdeutschlands und
1278 Vergleiche mit benachbarten Gebieten. Tübinger Mikropaläontologische Mitteilungen 3, pp. 232.

1279 Rimmer, S.M., Thompson, J.A., Goodnight, S.A., Robl, T.L., 2004. Multiple controls on the preservation of
1280 organic matter in Devonian-Mississippian marine black shales: geochemical and petrographic evidence.
1281 Palaeogeography, Palaeoclimatology, Palaeoecology 215, 125-154.

1282 Robinson, N., Eglinton, G., Brassell, S.C., Cranwell, P.A., 1984. Dinoflagellate origin for sedimentary 4α-
1283 methylsteroids and 5α(H)-stanols. Nature 308, 439-442.

1284 Röhl, H.J., Schmid-Röhl, A., Oschmann, W., Frimmel, A., Schwark, L., 2001. The Posidonia Shale (Lower
1285 Toarcian) of SW-Germany: an oxygen-depleted ecosystem controlled by sea level and palaeoclimate.
1286 Palaeogeography, Palaeoclimatology, Palaeoecology 165, 27-52.

1287 Rohmer, M., Bisseret, P., Neunlist, S., 1992. The hopanoids, prokaryotic triterpenoids and precursors of
1288 ubiquitous molecular fossils. In: Moldowan, J.M., Albrecht, P., Philp, R.P. (Eds.), Biological Markers in
1289 Sediments and Petroleum. Prentice Hall, Englewood Cliffs, N.J. pp. 1-17.

1290 Rullkötter, J., Wendisch, D., 1982. Microbial alteration of 17α(H) hopanes in Madagascar asphalts: removal of
1291 C-10 methyl group and ring opening. Geochim. Cosmochim. Acta 41, 1341-1353.

1292 Sabatino, N., Neri, R., Bellanca, A., Jenkyns, H.C., Baudin, F., Parisi, G., Masetti, D., 2009. Carbon-isotope
1293 records of the Early Jurassic (Toarcian) Oceanic Anoxic Event from the Valdorbia (Umbria-Marche
1294 Apennines) and Monte Mangart (Julian Alps) sections: palaeoceanographic and stratigraphic
1295 implications. Sedimentology 56, 1307-1328.

1296 Sabatino, N., Vlahović, I., Jenkyns, H.C., Scopelliti, G., Neri, R., Prtoljan, B., Velić, I., 2013. Carbon-isotope
1297 record and palaeoenvironmental changes during the early Toarcian oceanic anoxic event in shallow-
1298 marine carbonates of the Adriatic Carbonate Platform in Croatia. Geological Magazine 150, Issue 6,
1299 1085-1102.

1300 Sælen, G., Doyle, P., Talbot, M.R., 1996. Stable-isotope analysis of belemnite rostra from the Whitby Mudstone
1301 Fm., England: Surface water conditions during deposition of a marine black shale. Palaios 11, 97-117.

1302 Schlager, W., Schöllnberger, W., 1973. Das Prinzip stratigraphischer Wenden in der Schichtfolge der Nördlichen
1303 Kalkalpen. Mitt. Geol. Ges. Wien 66, 166-193.

1304 Schmid-Röhl, A., Röhl, H.-J., Oschmann, W., Frimmel, A., Schwark, L., 2002. Palaeoenvironmental
1305 reconstruction of Lower Toarcian epicontinental black shales (Posidonia Shale, SW Germany): global
1306 versus regional control. Geobios 35, 13-20.

1307 Schwark L., Vliex, M., Schaeffer, P., 1998. Geochemical characterization of Malm Zeta laminated carbonates
1308 from the Franconian Alb, SW Germany (II). Organic geochemistry 29, No. 8, 1921-1952.

1309 Schwark, L., Frimmel, A., 2004. Chemostratigraphy of the Posidonia Black Shale, SW Germany II. Assessment
1310 of extent and persistence of photic-zone anoxia using aryl isoprenoids distributions. Chem. Geol. 206,
1311 231-248.

1312 Sell, B., Ovtcharova, M., Guex, J., Bartolini, A., Jourdan, F., Spangenberg, J.E., Vicente, J.-C., Schaltegger, U.,
1313 2014. Evaluating the temporal link between the Karoo LIP and climatic-biologic events of the Toarcian
1314 Stage with high-precision U-Pb geochronology. Earth and Planetary Science Letters 408, 48-56.

1315 Sinninghe Damsté, J.S., Kock-Van Dalen, A.C., de Leeuw, J.W., Schenk, P.A., Guoying, S., Brassell, S.C.,
1316 1987. The identification of mono-, di-, and trimethyl 2-methyl-2-(4,8,12-trimethyltridecyl)chromans and
1317 their occurrence in geosphere. Geochimica et Cosmochimica Acta 51, 2393-2400.

1318 Sinninghe Damsté, J.S., van Duin, A.C.T., Hollander, D., Kohnen, M.E.L., de Leeuw, J.W., 1995. Early
1319 diagenesis of bacteriohopanepolyol derivatives: Formation of fossil homohopanoids. Geochimica et
1320 Cosmochimica Acta 59, 5141-5156.

1321 Spieler, A., Brandner, R., 1989. Vom jurassischen Pull-Apart Becken zur Westüberschiebung der Achentaler
1322 Schubmasse (Tirol, Österreich). Geol. Paläont. Mitt. Innsbruck 16, 191-194.

1323 Suan, G., Pittet, B., Bour, I., Mattioli, E., Duarte, L.V., Mailliot, S., 2008. Duration of the Early Toarcian carbon
1324 isotope excursion deduced from spectral analysis: consequence for its possible causes. Earth Planet. Sci.
1325 Lett. 267, 666-679.

1326 Summons, R.E., Powell, T.G., 1986. Chlorobiaceae in Palaeozoic seas revealed by biological markers, isotopes
1327 and geology. Nature 319, 763-765.

1328 Svensen, H., Planke, S., Chevalier, L., Malthe-Sørensen, A., Corfu, F., Jamveit, B., 2007. Hydrothermal venting
1329 of greenhouse gases triggering Early Jurassic global warming. Earth and Planetary Science Letters 256,
1330 554-566.

1331 Svensen, H., Corfu, F., Polteau, S., Hammer, Ø., Planke, S., 2012. Rapid magma emplacement in the Karoo
1332 Large Igneous Province. Earth Planet. Sci. Lett. 325–326, 1–9.

1333 Taylor, G.H., Teichmüller, M., Davis, A., Diessel, C.F.K., Littke, R., Robert, P., 1998. Organic Petrology, Gebr.
1334 Borntraeger, Berlin & Stuttgart, 704 p.

1335 ten Haven, H.L., de Leeuw, J.W., Peakman, T.M., Maxwell, J.R., 1986. Anomalies in steroid and hopanoid
1336 maturity indices. Geochimica et Chosmochimica Acta 50, 853-855.

1337 ten Haven, H.L., de Leeuw, J.W., Rullkötter, J., Sinninghe Damsté, J.S., 1987. Restricted utility of the pristane /
1338 phytane ratio as a palaeoenvironmental indicator. Nature 330, 641-643.

1339 ten Haven, H.L., de Leeuw, J.W., Schenk, P.A., 1985. Organic geochemical studies of a Messinian evaporitic
1340 basin, northern Appenines (Italy): Hydrocarbon biological markers for a hypersaline environment.
1341 Geochim. Cosmochim. Acta 49, 2181-2191.

1342 Thomas, H., Schiettecatte, L.-S., Suykens, K., Kone, Y.J.M., Shadwick, E.H., Prowe, A.E.F., Bozec, Y., de Baar,
1343 H.J.W., Borges, A.V., 2008. Enhanced ocean carbon storage from anaerobic alkalinity generation in
1344 coastal sediments. Biogeosciences Discuss. 5, 3575-3591.

1345 Tissot, B.T., Welte, D.H., 1984. Petroleum Formation and Occurrences, Second Ed. Springer-Verlag, Berlin. pp.
1346 699.

1347 Tollmann, A., 1976. Analyse des klassischen nordalpinen Mesozoikums. Stratigraphie, Fauna und Fazies der
1348 Nördlichen Kalkalpen. Deuticke, Wien, pp. 580.

1349 Tollmann, A., 1985. Geologie von Österreich, Band 2. Deuticke, Wien, pp. 718.

1350 Tsikos, H., Jenkyns, H.C., Walsworth-Bell, B., Petrizzo, M.R., Forster, A., Kolonic, S., Erba, E., Premoli Silva,
1351 I., Baas, M., Wagner, T., Sinninghe Damsté, J.S., 2004. Carbon-isotope stratigraphy recorded by the
1352 Cenomanian–Turonian Oceanic Anoxic Event: correlation and implications based on three key localities.
1353 J. Geol. Soc. Lond. 161, 711-719

1354 Tyson, R.V., 1995. Sedimentary Organic Matter - Organic Facies and Palynofacies. Chapman and Hall, London.

1355 van de Schootbrugge, B., McArthur, J.M., Bailey, T.R., Rosenthal, Y., Wright, J.D., Miller, K.G., 2005.
1356 Toarcian anoxic event: An assessment of global using belemnite C isotope records. Paleoceanography 20,
1357 PA3008, doi:10.1029/2004PA001102.

1358 Volkman, J.K., Maxwell, J.R., 1986. Acyclic isoprenoids as biological markers. In: Johns, R.B. (Eds.),
1359 Biological Markers in the Sedimentary Record. Elsevier, Amsterdam. pp. 1-42.

1360 Volkman, J.K., Kearney, P., Jeffrey, S.W., 1990. A new source of 4-methyl steroids and 5α(H)-stanols in
1361 sediments: prymnesiophyte microalgae of the genus Pavlova. Organic Geochemistry 15, 489-497.

1362 Volkman, J.K., Barrett, S.M., Blackburn, S.I., 1999. Eustigmatophyte microalgae are potential sources of $C_{29}$
1363 sterols, $C_{22}$-$C_{28}$ n-alcohols and $C_{28}$-$C_{32}$ n-alkyl diols in freshwater environments. Organic Geochemistry
1364 30, 307-318.

1365 Vortisch, W., 1982. Clay mineralogical studies of some tills in northern Germany. Geologica et Palaeontologica
1366 15, 167-192.

1367 Watson, J.S., Jolley, D.W., Kelly, S.P., 2009. High concentration of 28,30-bisnorhopane and 25,28,30-
1368 trisnorhopane at the PETM in the Faroe-Shetland basin. In: 24th International Meeting on Organic
1369 Geochemistry, 6-11 September 2009. Bremen, Germany.

1370 Weissert, H., 2000. Deciphering methane's fingerprint. Nature 406, 356-357.

1371 Weissert, H., 2013. C-isotope geochemistry – tool for chemostratigraphy and carbon cycle history. Ciencias da
1372 terra 18.

Whiteside, J.H., Olsen, P.E., Kent, D.V., Fowell, S.J., Et-Touhami, M., 2007. Synchrony between the Central Atlantic magmatic province and the Triassic-Jurassic mass extinction event? Palaeogeography, Palaeoclimatology, Palaeoecology 244, 345-367.

Wignall, P.B., Newton, R.J., Little, C.T.S., 2005. The timing of paleoenvironmental change and cause-and-effect relationships during the Early Jurassic mass extinction. Europ. American Journal of Science 305, 1014-1032.

## Figure captions

Fig. 1: (A) Schematic tectonic map of the Eastern Alps after Frisch and Gawlick (2003). The position of the studied section in the Bächental valley is indicated. (B) Palaeogeographic position of the study section as part of the Northern Calcareous Alps within the Austroalpine domain in late Early Jurassic time (after Frisch, 1979; Golonka, 2002; Vlahović et al., 2005; Gawlick et al., 2008; Bernoulli and Jenkyns, 2009; Missoni and Gawlick, 2011). The Northern Calcareous Alps are part of a continent between the Alpine Atlantic Ocean to the northwest and the Neotethys Ocean to the east/southeast. Formation of oceanic crust started in the late Early Jurassic (Ratschbacher et al., 2004). (C) Schematic cross section (for position, see line a-b in Fig. 1.B) showing the passive continental margin of the Lower Austroalpine domain (e.g., Frisch, 1979; Tollmann, 1985, Faupl & Wagreich, 2000; Gawlick et al., 2009; Frisch et al., 2011). Rifting and spreading of the Alpine Atlantic commencing in the late Early Jurassic affected the Austroalpine domain by the formation of extensional basins (horst-and-graben structure, asymmetric basins; cf. Bernoulli and Jenkyns, 1974). (D) Paleogeography of the depositional area of Bächental bituminous marl in the Lower Jurassic (Spieler and Brandner, 1989; Brandner, 2011). The accumulation of organic-rich rocks was restricted to the deepest parts of a basin with half-graben geometry. (E) Photograph of the outcropping Bächental bituminous marl in the open pit.

Fig. 2: Left: Lithological profile of the investigated Bächental section containing rocks of the *Scheibelberg Fm.*, the *Sachrang Member* (*Middle Allgäu Fm.*) and the *Upper Allgäu Fm*. Stratigraphy follows the new data gained within this study premised on the occurrence of *Cleviceras exaratum* and the comparison of

$C_{27}/C_{29}$ steranes ratios. Positions of the 68 investigated samples and the differentiated units are indicated (see text for explanations). Right: Photographs of thin sections: (A) Greyish wackestone with mainly radiolarians and subordinated *Bositra*, sponge spicules, ostracods and some foraminifera; secondary carbonates are abundant (Unit 1; 5.05 m). (B) Finely laminated mudstone containing some low-energy carbonatic turbidites (Subunit 2a; 13.39 m). (C) Radiolarian wackestone (Subunit 2a; 19.15 m). (D) Mudstone with frequent carbonate turbidites directly below the debrite (Subunit 2b; 21.55 m). (E) Wackestone (Unit 3; 29.45 m) with similar features as (A). Positions of the samples are displayed next to the lithological profile.

Fig. 3: Vertical variation of (A) protodolomite (peak area), (B) total organic carbon (TOC, %), (C) calcite equivalent (Cceq, %), (D) sulphur content (S, %), (E) hydrogen index (HI, mg HC/g TOC) for samples of the study section. The distinguished units within the Bächental bituminous marl are highlighted. See text for explanations.

Fig. 4: Vertical variation of (A) iron concentration (Fe, %), (B) inorganic carbon isotope composition ($\delta^{13}C_{carb}$, ‰ VPDB), (C) oxygen isotope composition of carbonate ($\delta^{18}O_{carb}$, ‰ VPDB), (D) organic carbon isotope composition ($\delta^{13}C_{org}$, ‰ VPDB) for samples of the study section. The distinguished units within the Bächental bituminous marl are highlighted. See text for explanations.

Fig. 5: Microphotographs of Bächental bituminous marls (A) Sample BT 15 (Unit 1, 7.65 m), (B) sample BT 25 (Subunit 2a, 13.39 m), (C) BT 44 (Unit 3, 22.60 m), and (D) BT 58 (Unit 3, 29.45 m). All photos under UV light.

Fig. 6: Total ion current gas chromatograms of saturated hydrocarbon fractions: (A) sample BT 15 (Unit 1; 7.65 m), (B) sample BT 25 (Subunit 2a; 13.39 m), (C) sample BT 30 (Subunit 2a; 16.55 m), (D) sample BT 50 (Unit 3; 25.55 m). *n*-alkanes are labelled according to carbon number [Std., standard (deuterated n-tetracosane)].

Fig. 7: Vertical variation of (A) *n*-alkane proportions of low (*n*-$C_{15-19}$) and high (*n*-$C_{27-31}$) molecular weight relative to the concentration of total *n*-alkanes (Σ*n*-alkanes), (B) concentration ratio of pristane vs. phytane, (C) concentration ratios of $C_{27}/C_{29}$ ααα*R* steranes and $C_{27}/C_{29}$ steranes, (D) concentration ratios of 4-methylsteranes/Σ$C_{29}$ steranes and mono- vs. triaromatic steroids, (E) concentration ratios of [20S/(20S + 20R)] $C_{29}$ steranes and dibenzothiophene vs. phenantrene (DBT/Phen), (F) concentration ratios of gammacerane index and [22S/(22S + 22R)] isomers of $C_{31}$ hopane for bituminous marl samples. The distinguished units within the Bächental bituminous marl are highlighted. See text for explanations.

Fig. 8: Partial mass chromatograms of steranes (m/z 217) and 4-methylsteranes (m/z 231) in saturated hydrocarbon fractions of (A) sample BT 15 (Unit 1; 7.65 m), (B) sample BT 25 (Subunit 2a; 13.39 m), (C) sample BT 30 (Subunit 2a; 16.55 m), (D) sample BT 50 (Unit 3; 25.55 m).

Fig. 9: Partial mass chromatograms of hopanes (m/z 191) in saturated hydrocarbon fractions of (A) sample BT 15 (Unit 1; 7.65 m), (B) sample BT 25 (Subunit 2a; 13.39 m), (C) sample BT 30 (Subunit 2a; 16.55 m), (D) sample BT 50 (Unit 3; 25.55 m). Variations of gammacerane and hopane isomerization are remarkable.

Fig. 10: The plot of pristane/phytane vs. dibenzothiophene/phenantrene (Pr/Ph vs. DBT/Phen) suggests the predominance of anoxic conditions during deposition of Subunit 2a and a shift to less reducing conditions in Subunit 2b. In contrast, suboxic conditions prevailed during deposition of Units 1 and 3. Modified after Didyk et al. (1978) and Hughes et al. (1995).

Fig. 11: Ternary diagram (Fe-TOC-S) after Dean and Arthur (1989). Samples of Units 1 and 3 plot along the pyrite line and in the field of excess Fe availability suggesting suboxic to anoxic conditions during deposition. In contrast, the plot indicates Fe limitation and persistent anoxia in Unit 2.

Fig. 12: The plot of gammacerane indices vs. 4-methylsteranes/$\Sigma C_{29}$ steranes (GI vs. 4-methylsteranes/$\Sigma C_{29}$ steranes) indicates enhanced salinity of bottom waters and a stratified water column during deposition of samples from Subunit 2a whereas normal-marine salinity was prevailing during deposition of the remaining parts of the section. The well-defined positive correlation between GI and 4-methylsteranes suggest a flourishing of halophilic organisms during phases of enhanced salinity. Modified after Schwark et al. (1998) and Bechtel et al. (2012).

Fig. 13: Influence of sea-level changes on depositional environment and correlation of Pliensbachian to Toarcian OM-rich sediments of Alpine (Bächental) and epicontinental (Dotternhausen; Frimmel et al., 2004) settings with global sea-level curve (Haq et al., 1988) using sterane ratios. See text for explanations.

Fig. 14: Sketches showing factors controlling the depositional environment of the Bächental bituminous marl. Paleogeographical setting modified after Brandner (2011). (A) Units 1 and 3, (B) Subunit 2a, (C) Subunit 2b. See text for explanations.

**Figure 1**

**Click here to download high resolution image**

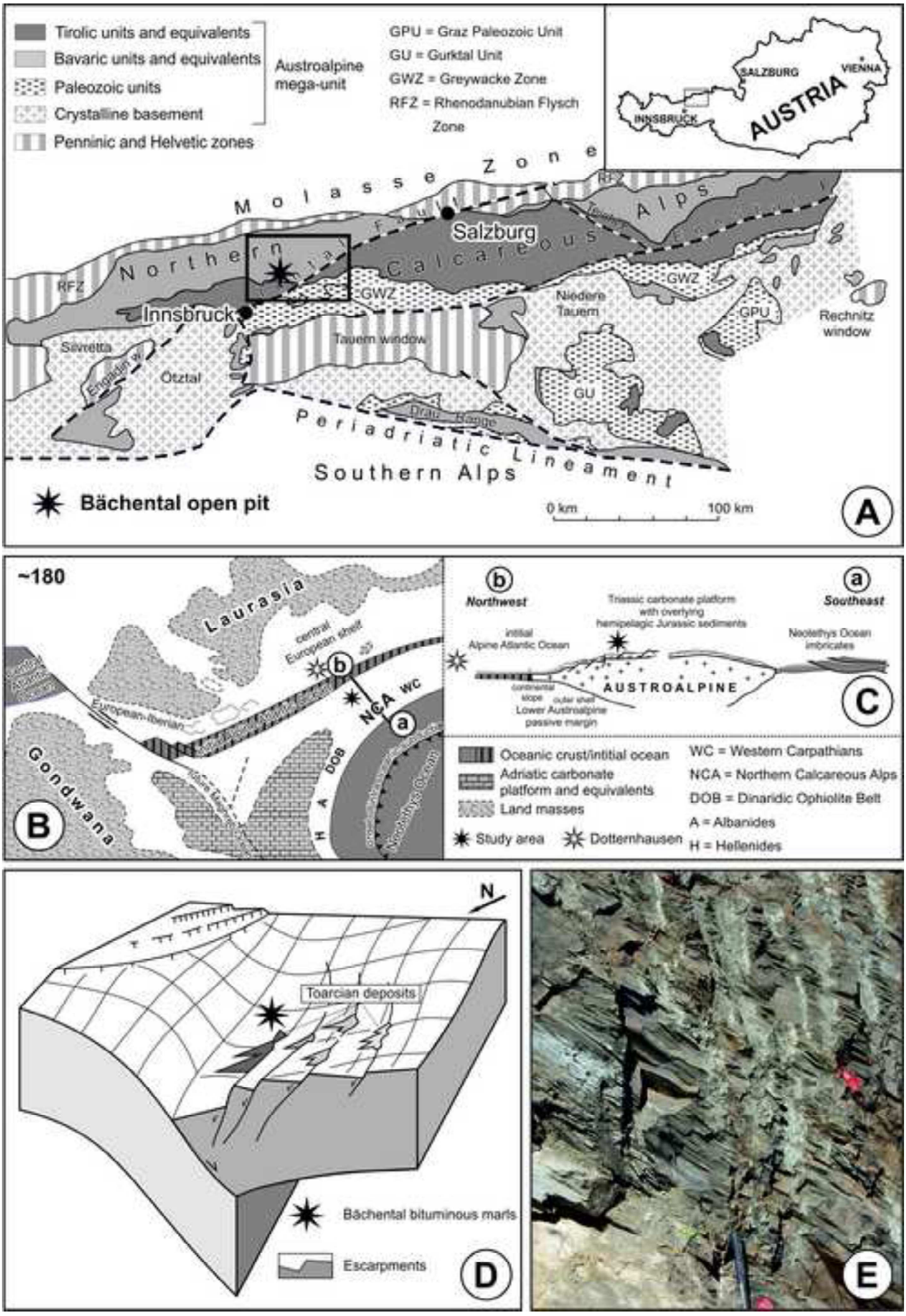

**Figure 2**

Click here to download high resolution image

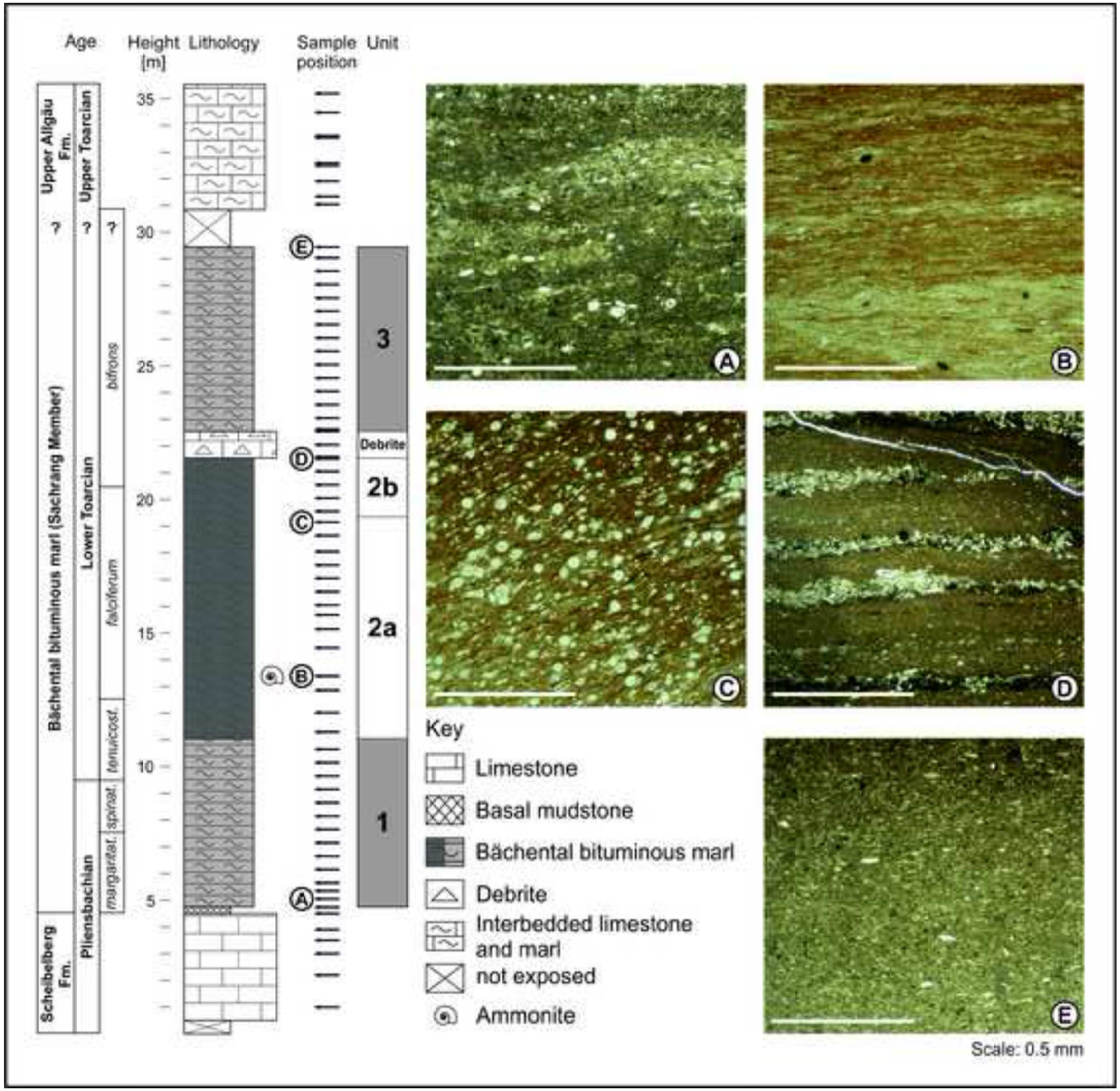

**Figure 3**

**Click here to download high resolution image**

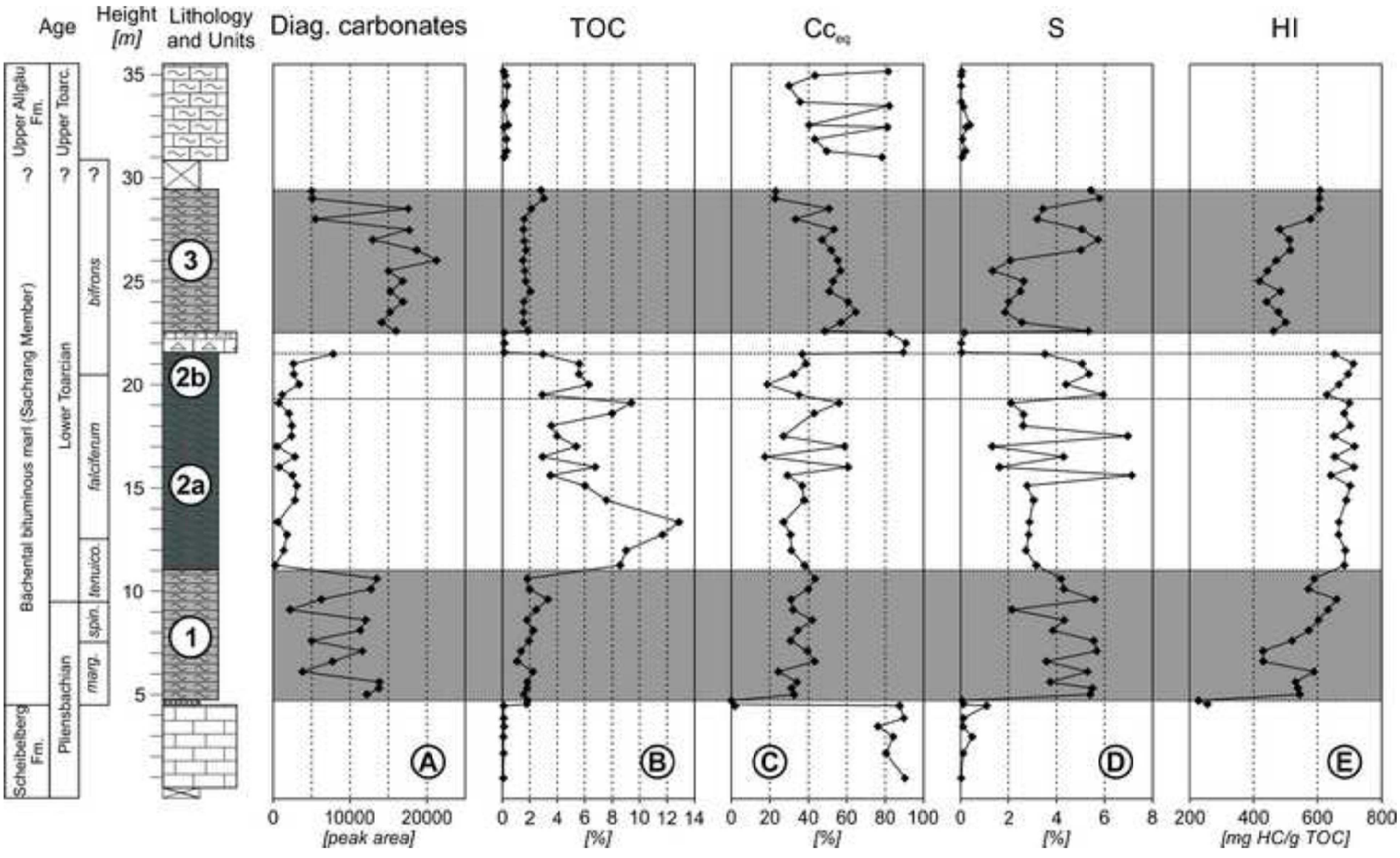

**Figure 4**

Click here to download high resolution image

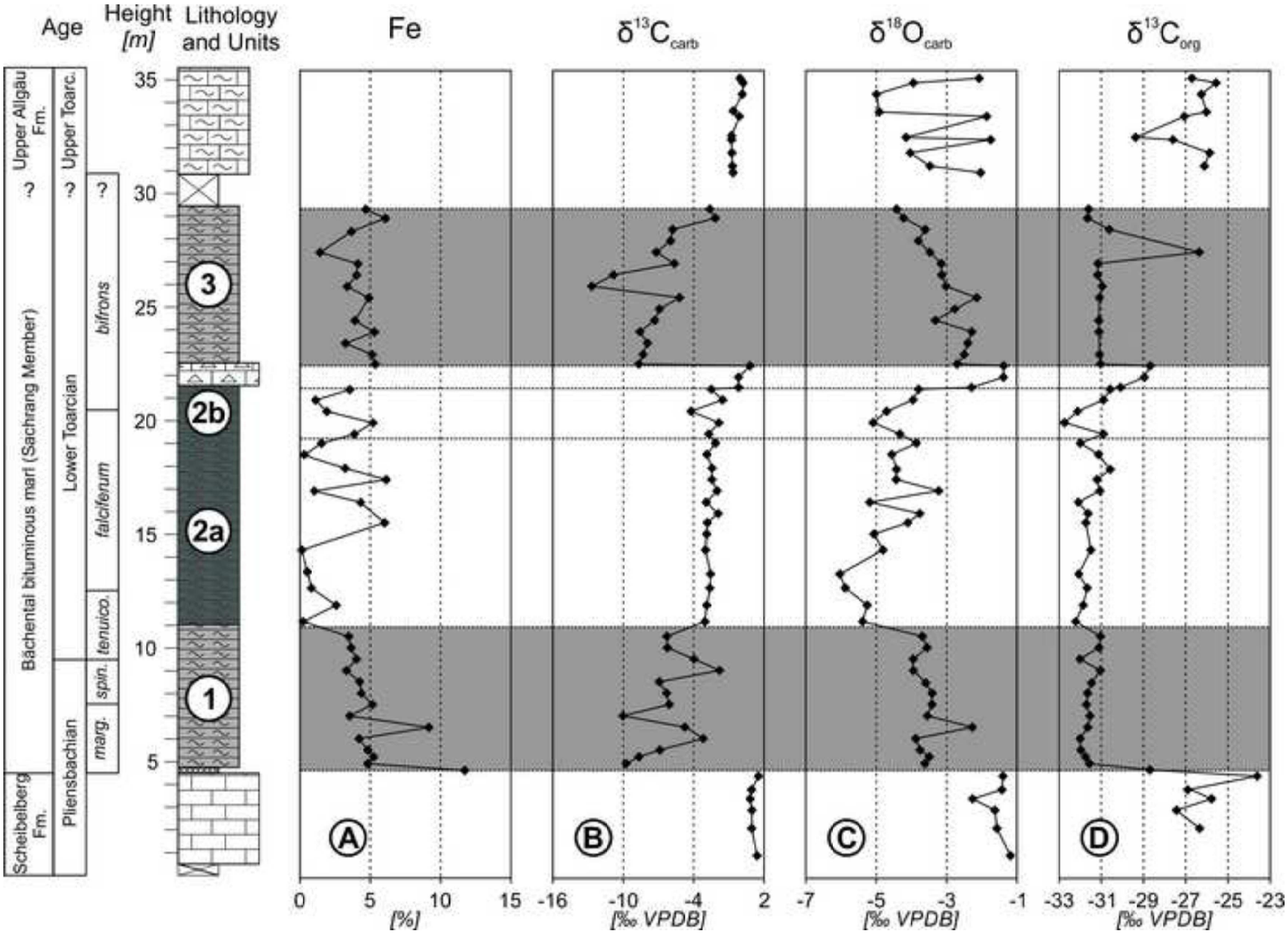

**Figure 5**
**Click here to download high resolution image**

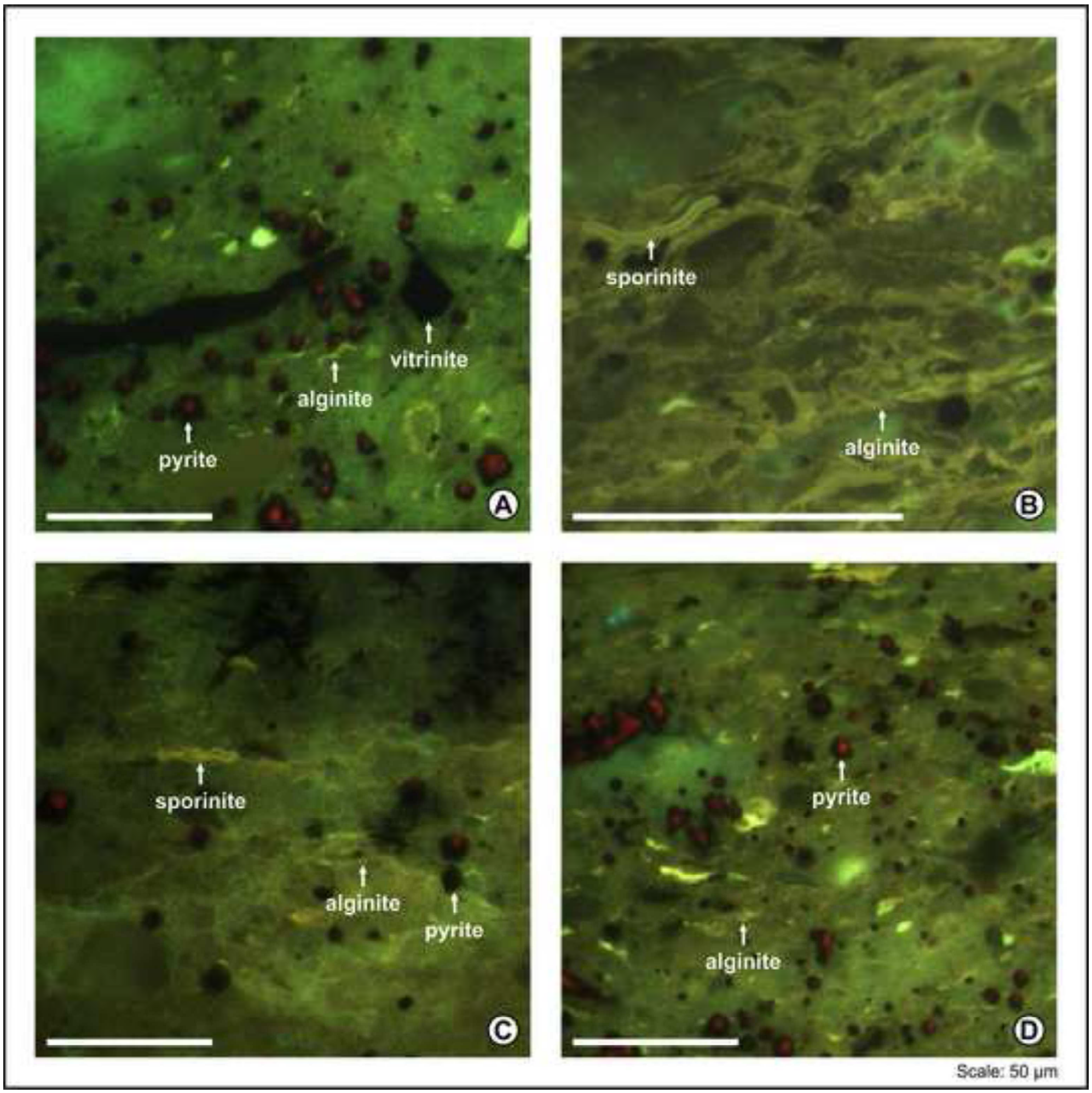

**Figure 6**

**Click here to download high resolution image**

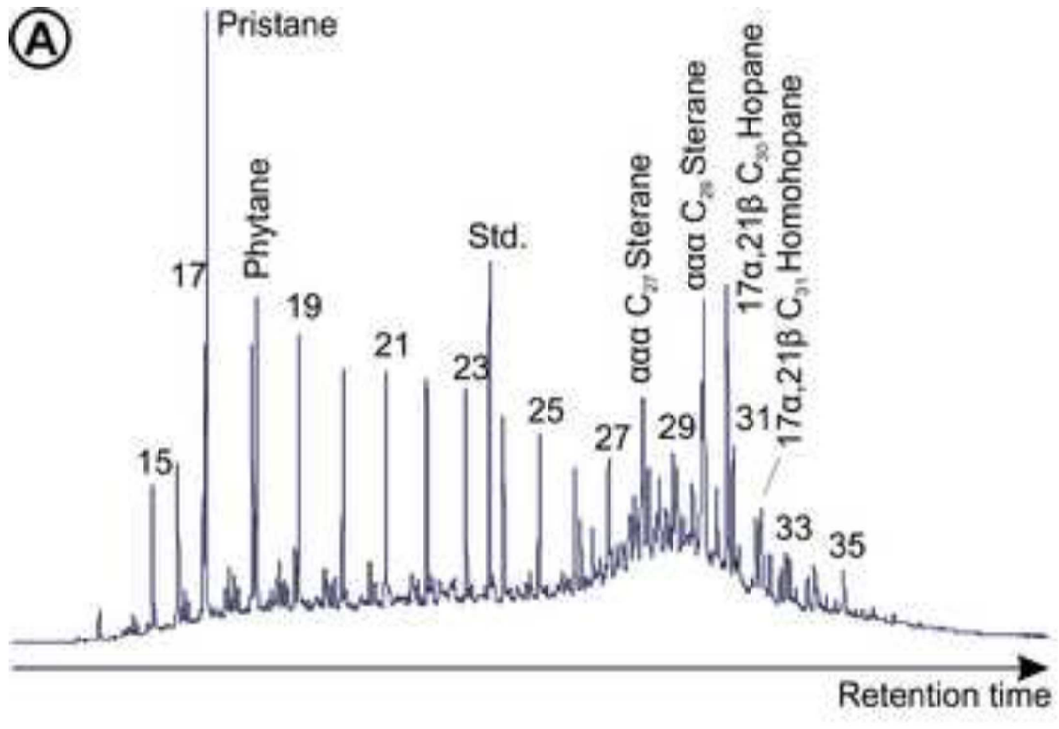


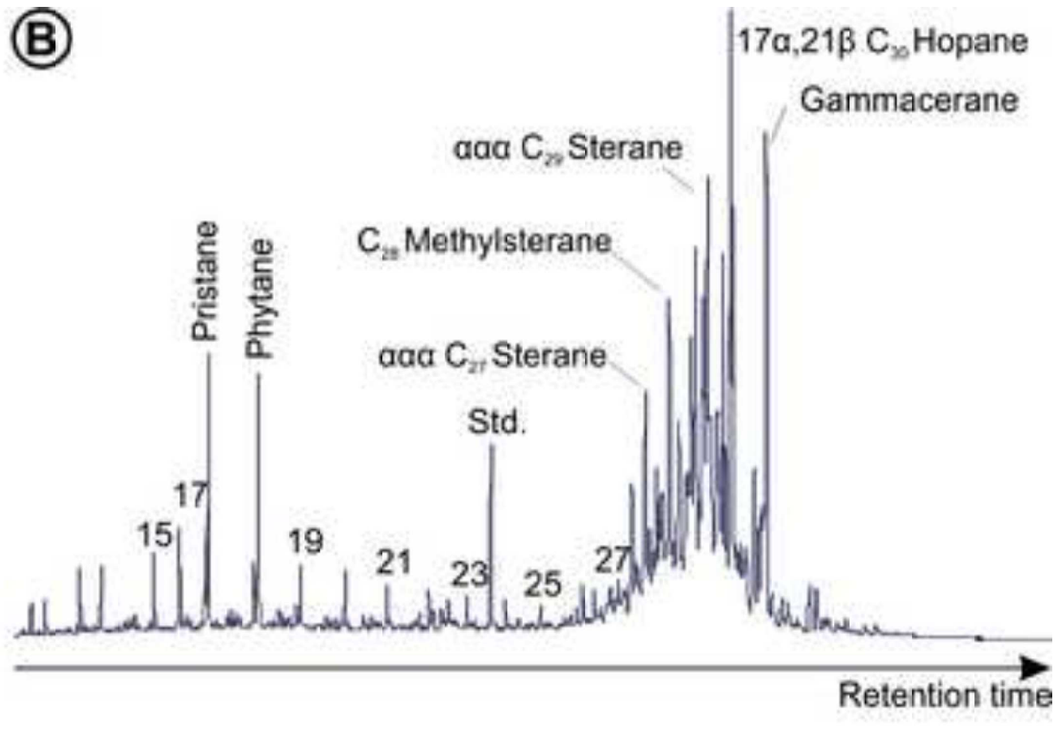


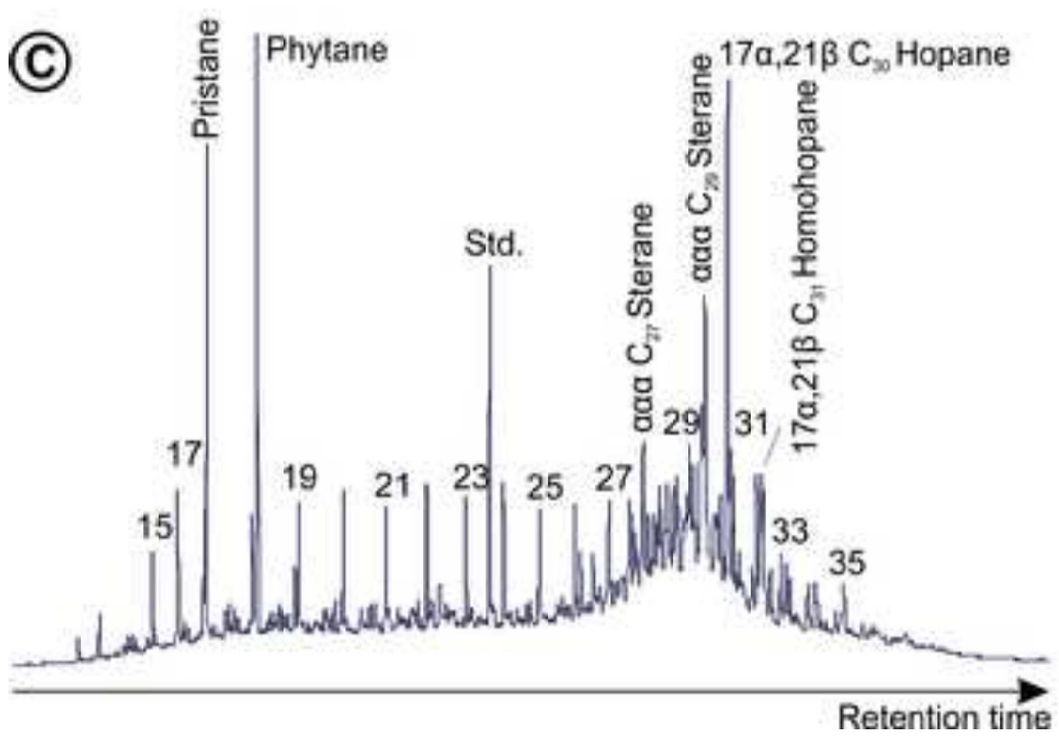


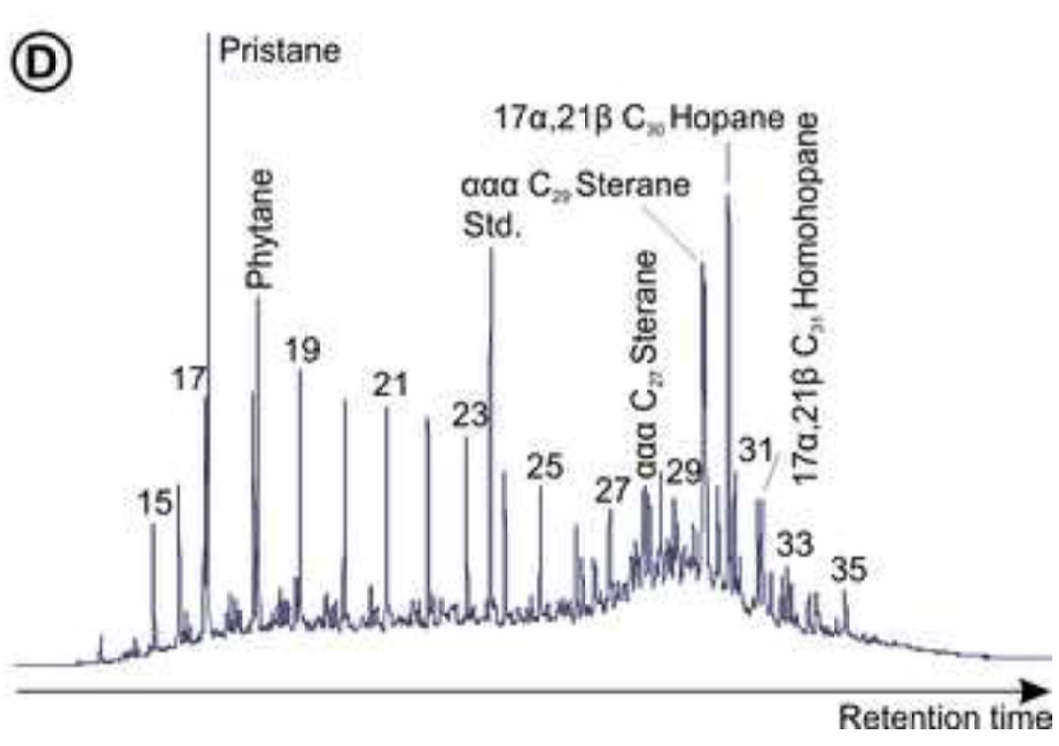

**Figure 7**
**Click here to download high resolution image**

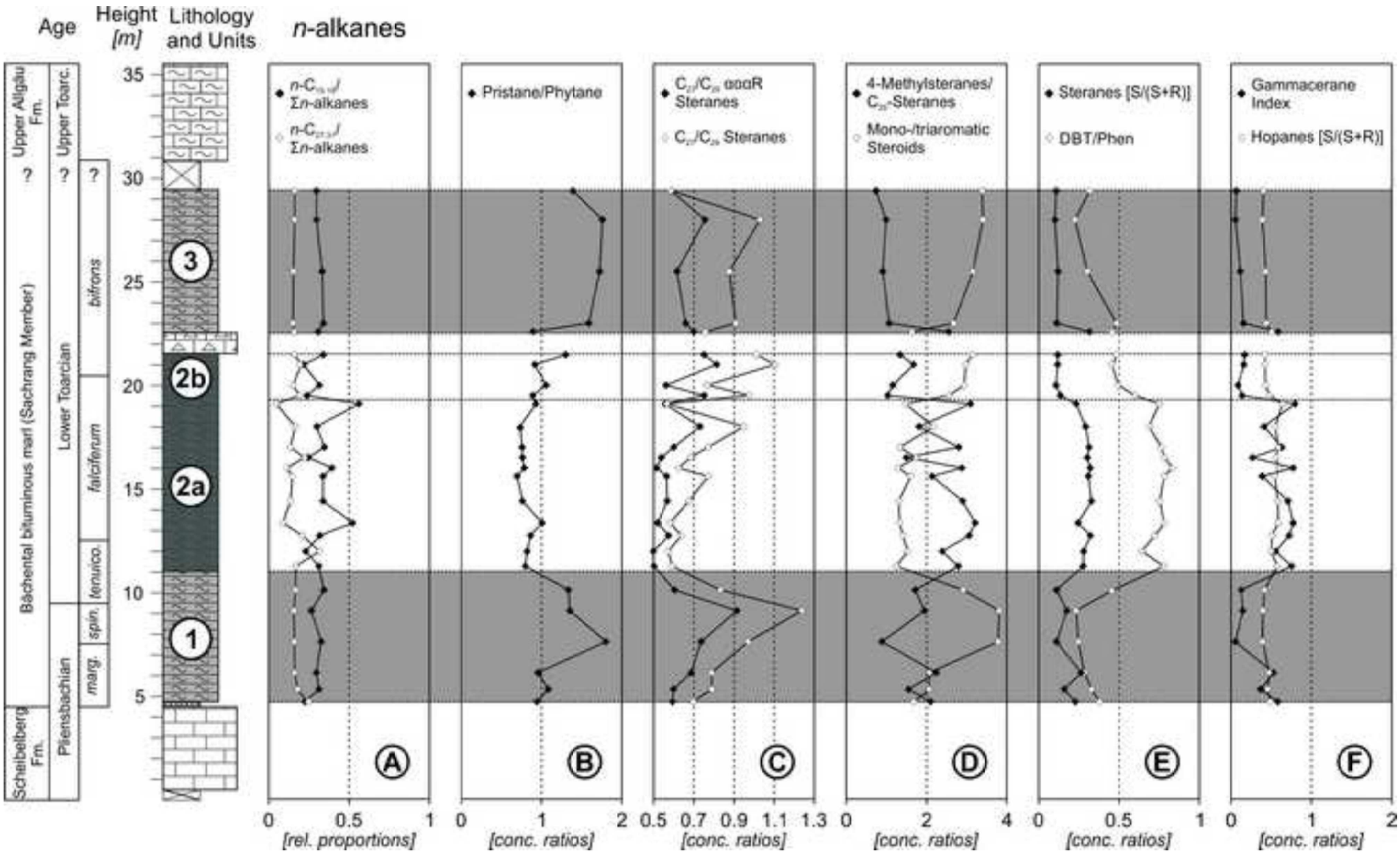

**Figure 8**

Click here to download high resolution image

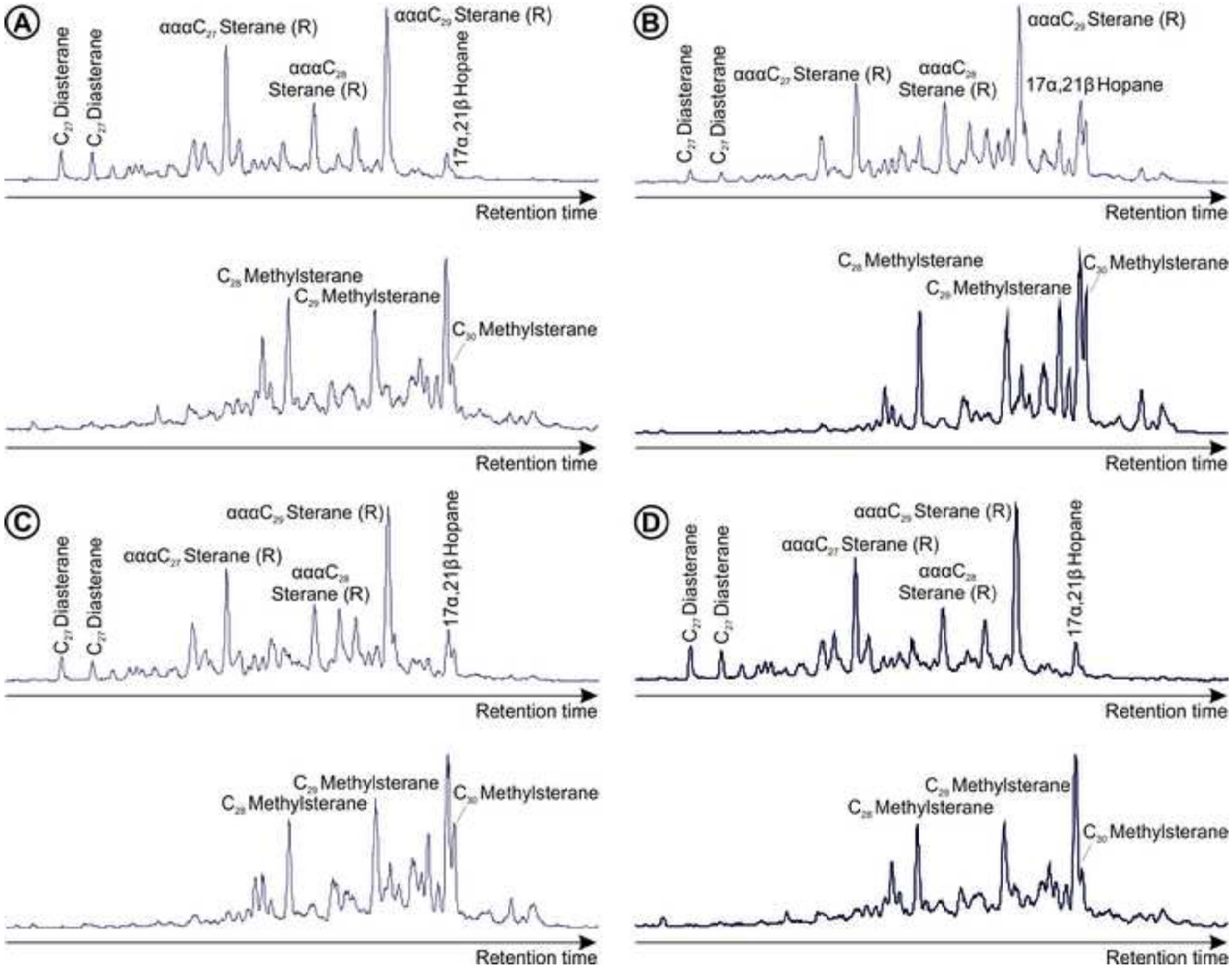

**Figure 9**

Click here to download high resolution image

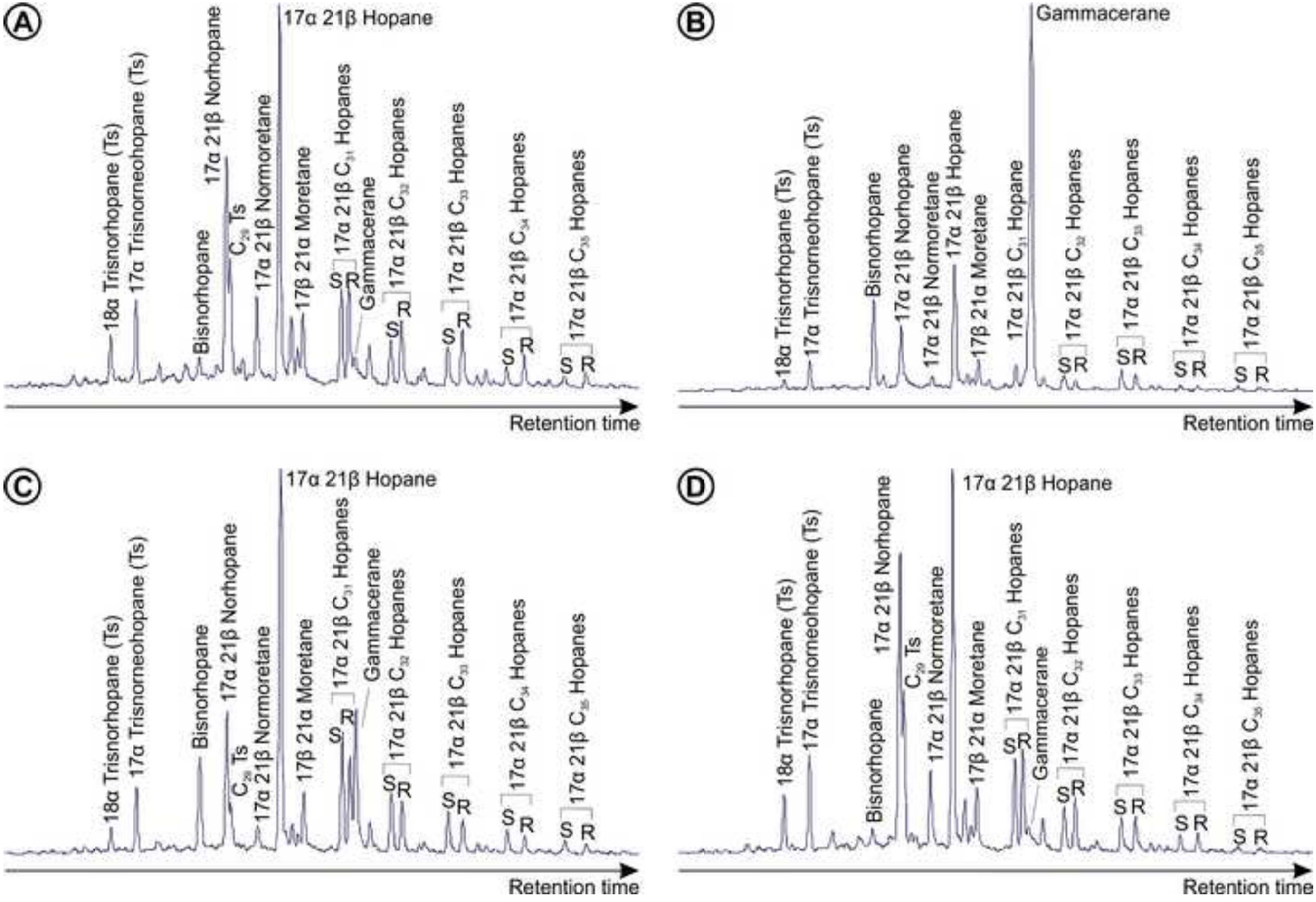

**Figure 10**
**Click here to download high resolution image**

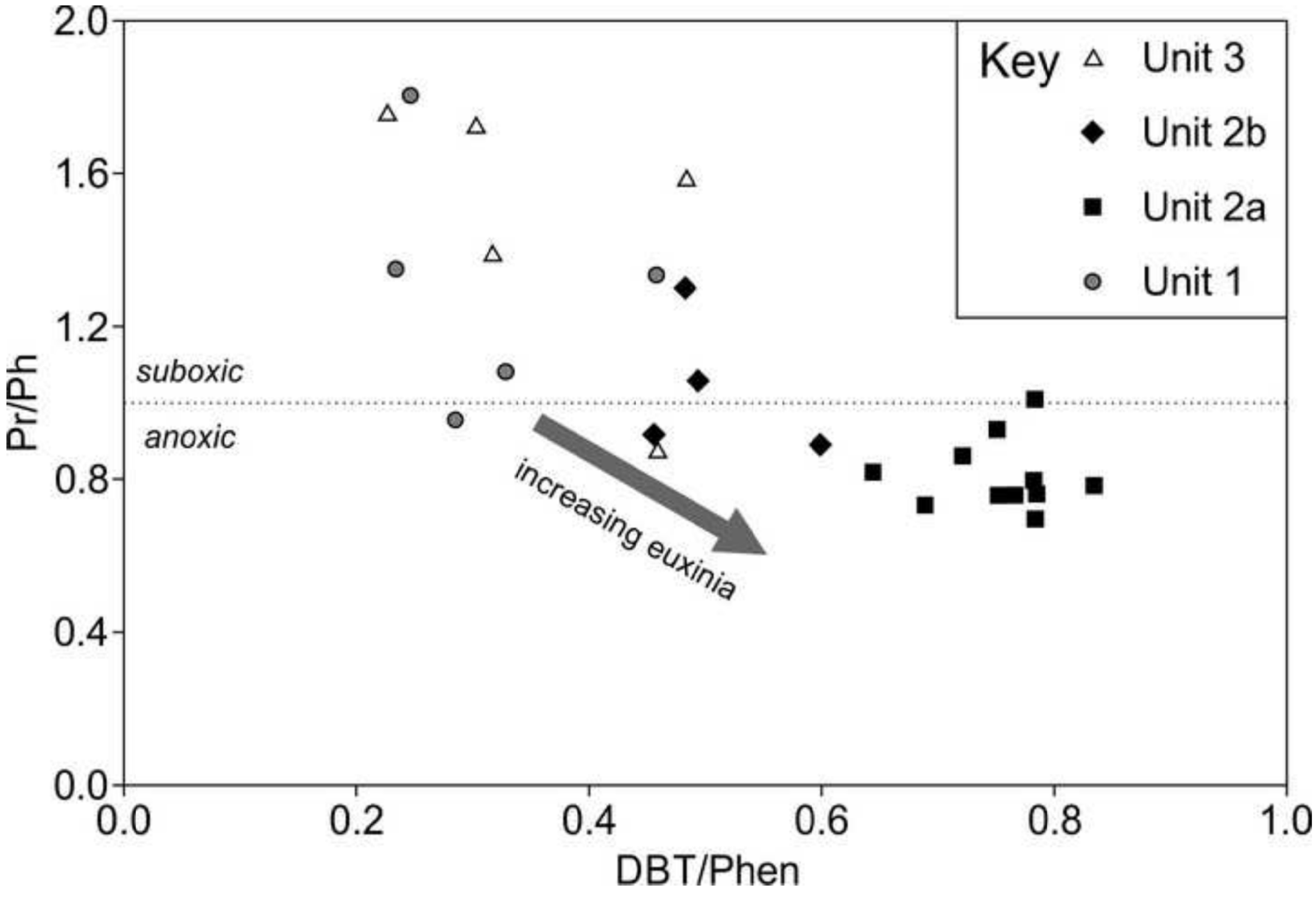

**Figure 11**
**Click here to download high resolution image**

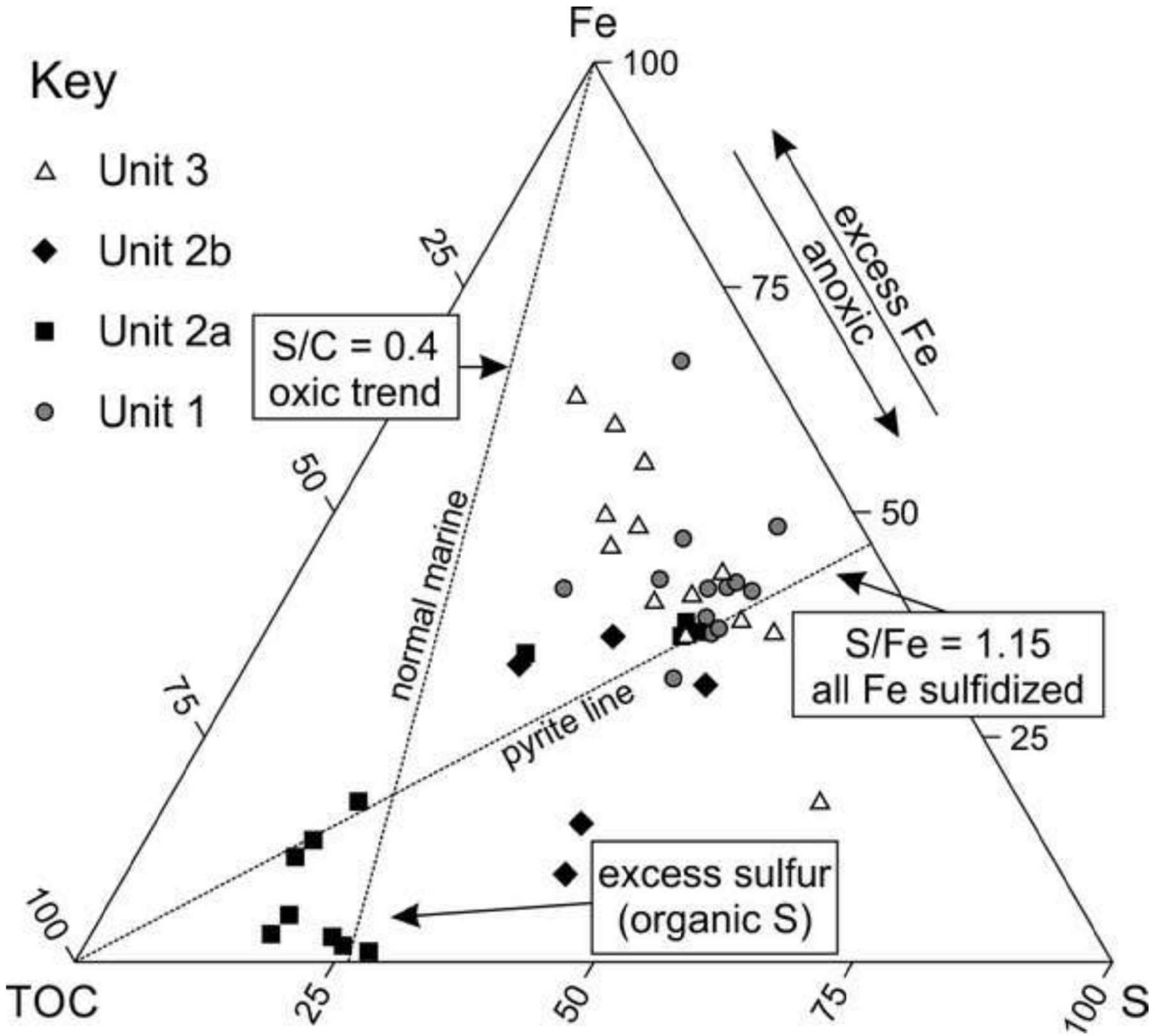

**Figure 12**
**Click here to download high resolution image**

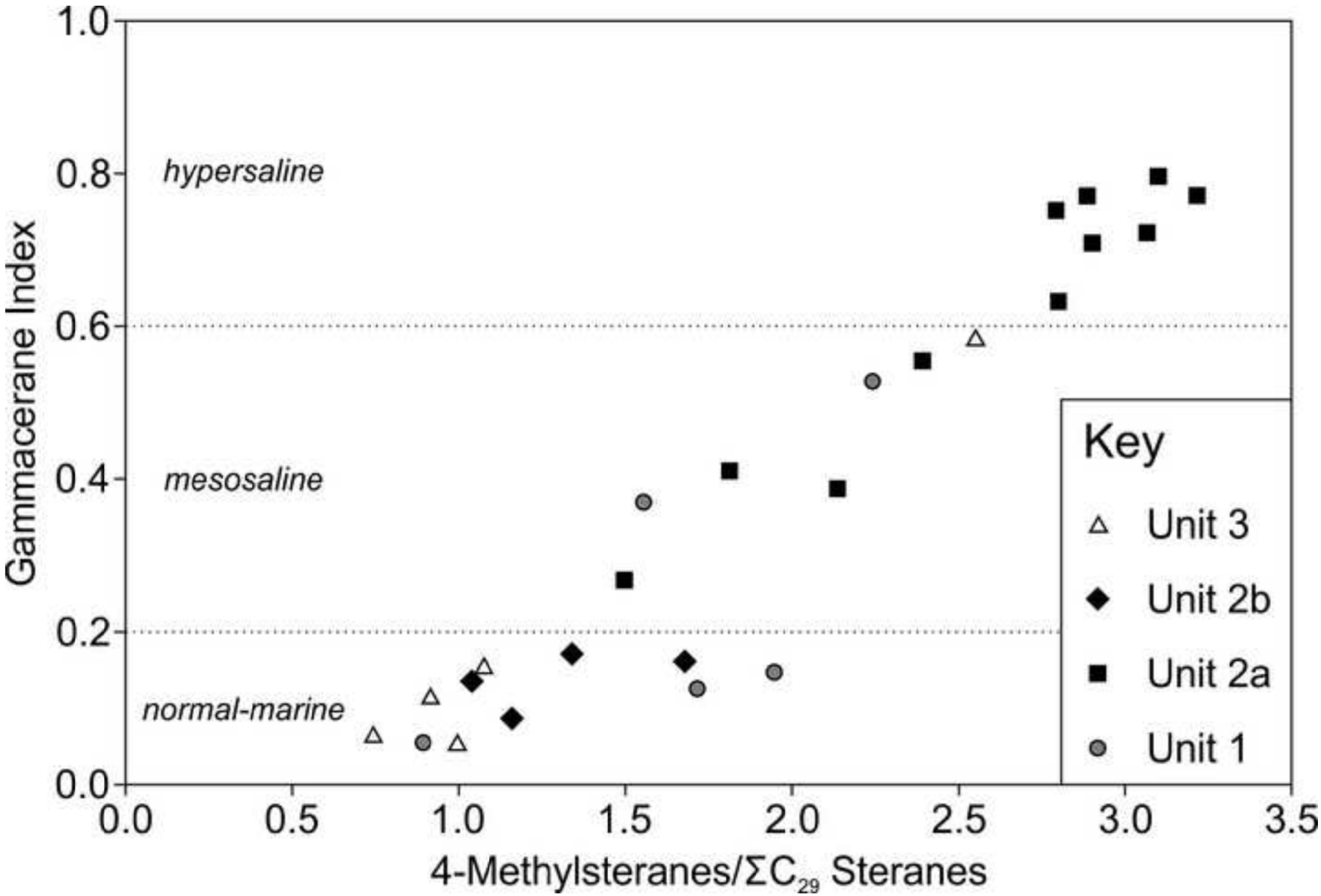

**Figure 13**

**Click here to download high resolution image**

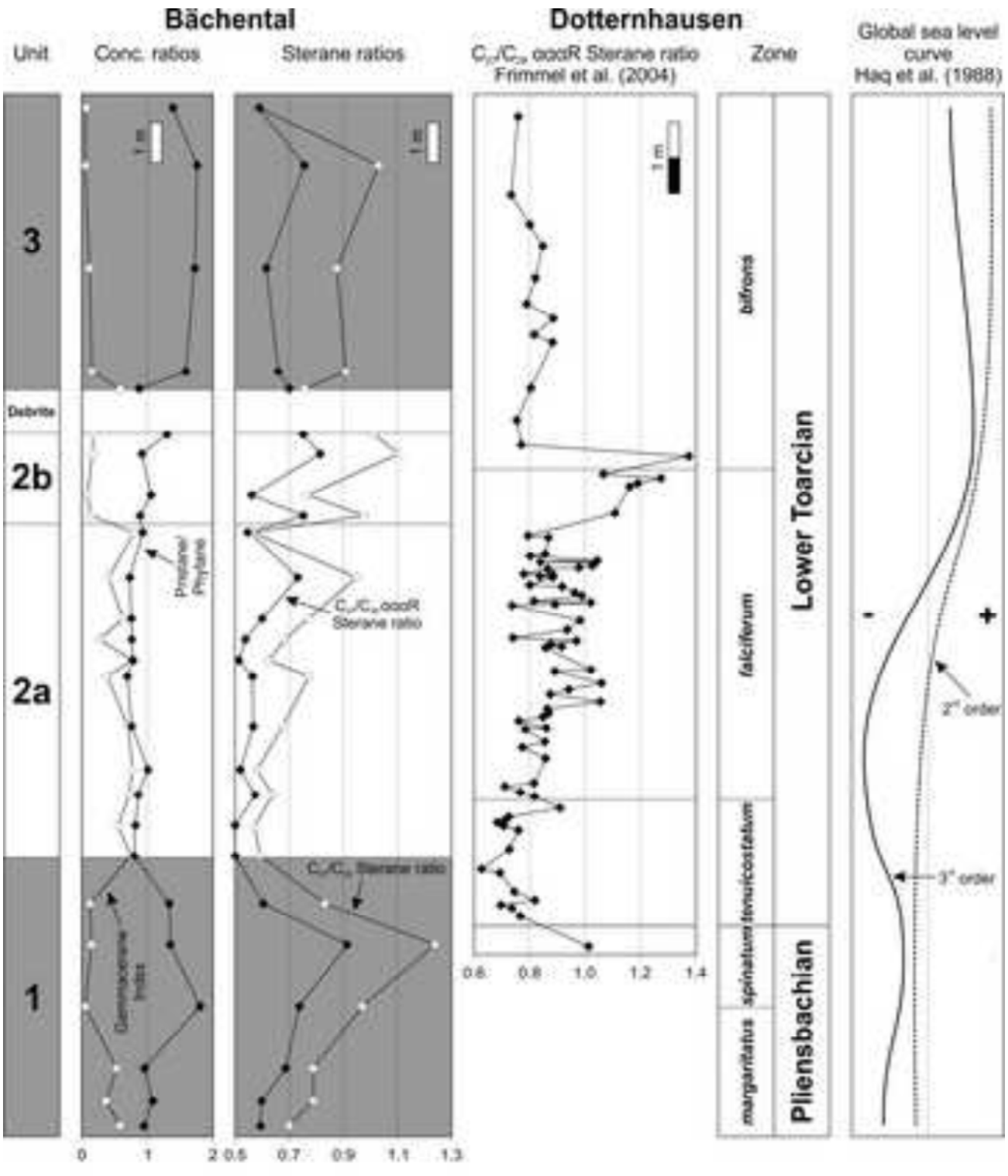

**Figure 14**

**Click here to download high resolution image**